Polymer Chemistry

ROYAL SOCIETY OF CHEMISTRY

PAPER

View Article Online
View Journal | View Issue

Cite this: *Polym. Chem.*, 2024, **15**, 661

Pillar[5]arene-based dually crosslinked supramolecular gel as a sensor for the detection of adiponitrile†

Maksim Rodin, David Helle and Dirk Kuckling*

Received 8th December 2023,
Accepted 10th January 2024

DOI: 10.1039/d3py01354e

rsc.li/polymers

Host–guest inclusion complex formation between pillar[5]arene (P5A) and various guest molecules (amine- and heterocycle-substituted *N*-Boc-aminohexanes) in $CDCl_3$ was investigated using NMR titration as well as 2D NMR (NOESY and DOSY) techniques. Supramolecular complexes with methylimidazolium (MIHA) and pyridinium substituted guests were demonstrated to have the highest binding affinity towards P5A ($\log K_a$ = 3.32 ± 0.10, 3.66 ± 0.09, respectively). Dimethyl acrylamide-2-vinyl-4,4-dimethyl azlactone copolymer was modified with mono-substituted P5A and MIHA as well as a photocrosslinker based on 3,4-dimethyl maleimide to obtain host and guest polymers, which were combined and spin-coated onto a gold-coated quartz substrate to fabricate a dually crosslinked supramolecular gel (DCSG) containing reversible and irreversible crosslinks in a single network. Such DCSG chip was utilized as a sensor for the detection of adiponitrile (AN) in organic solutions based on a competitive complex formation with P5A. Macroscopic changes in the gel (*e.g.*, in swelling degree or in refractive index) upon presence of AN (1 μM–1 mM) in chloroform were monitored with surface plasmon resonance (SPR) spectroscopy. The limit of detection of AN using our platform was determined to be as low as 25 μM.

Introduction

Gels, *i.e.*, polymer chains interconnected *via* covalent crosslinking moieties into three-dimensional networks, represent one of the most important classes of synthetic materials.[1,2] Despite their versatility for numerous applications, such networks exhibit often insufficient mechanical properties and poor reversibility, which drastically limits the applicability of the gels. However, their fusion with supramolecular chemistry paved the way for numerous opportunities to enhance the properties of the gels, or even to endow the gels with unprecedented ones.[3,4] The introduction of supramolecular interactions (such as ionic interactions,[5–7] metal/ligand complexes,[8] hydrogen bonding[9,10] or host–guest inclusion complexes[11–13]) into the network results in the reversible crosslinks between the polymer chains. This, in turn, bestows the systems with improved mechanical properties[14] and susceptibility towards the changes in the medium and thus with stimuli-responsiveness. This feature is the key for the fabrication of smart materials that can be utilized in diverse areas ranging from tissue engineering,[15–18] bioelectronics,[19,20] and drug delivery[21–24] to self-healing materials,[25,26] actuators,[27–29] and sensors.[12,30,31]

Lately, the focus of various research groups has been shifted onto polymeric networks that combine multiple types of crosslinks in one system.[32,33] Utilization of dual reversible crosslinking, for instance, was shown to endow the networks with multi-stimuli-responsiveness as well as shape memory behavior.[34–37] Furthermore, incorporation of a covalent and a non-covalent linkage types in a single gel was demonstrated to be highly promising since it receives the advantages of both types:[38,39] the former provides an integrity of structure to the system, whereas the latter is responsible for the reversibility and responsiveness. Such combination proved to be beneficial for the fabrication of reusable devices, which is especially important in sensing applications. Recently, dually crosslinked hydrogel sensors were developed in our working group for the detection of small molecules[40] and ovarian cancer biomarker[41] – lysophosphatidic acid (LPA). Reversible crosslinks in a form of a host–guest complex with β-cyclodextrin were disrupted in the presence of an analyte – a compound with a higher binding affinity to cyclodextrin – which led to a decrease in the crosslink density and, therefore, to an increased swelling. The swelling behavior was monitored by SPR spectroscopy,[42] the sensitivity of which offered a limit of detection of the LPA as low as 0.122 μM.

Nitriles comprise a chemical substance family which is of high importance in various areas such as chemical industry

Department of Chemistry, Paderborn University, Warburger Str. 100, 33098 Paderborn, Germany. E-mail: dirk.kuckling@uni-paderborn.de

† Electronic supplementary information (ESI) available. See DOI: https://doi.org/10.1039/d3py01354e

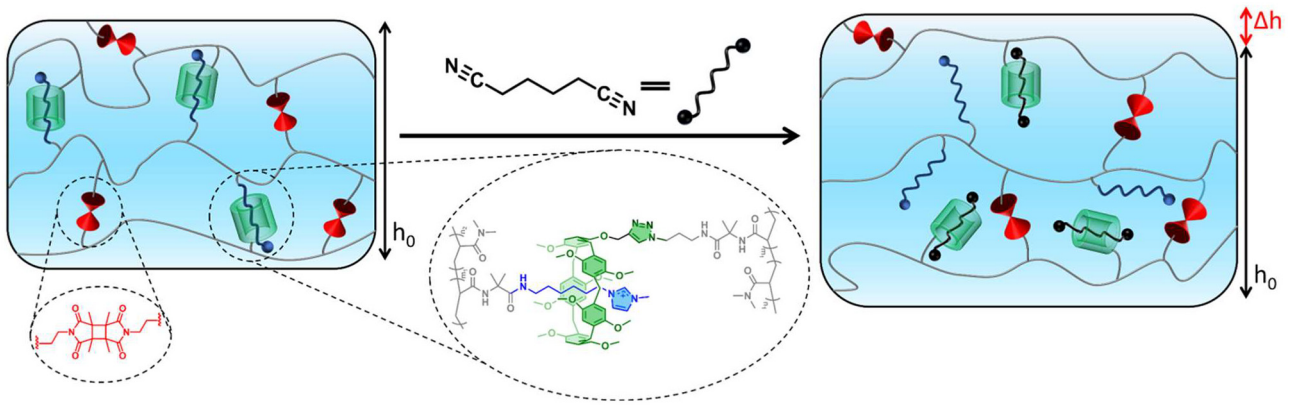

Fig. 1 The concept of a pillar[5]arene-based dually crosslinked gel sensor for the detection of adiponitrile.

(where they are extensively used as precursors for plastics, fibers, *etc.*[43,44]), or medicine (*e.g.*, as biomarkers of chemotherapy-related kidney damage in cancer patients[45]). In the field of chemical industry adiponitrile is one of the key members of the nitrile family. It is used in the synthesis of nylon-6,6, which is the reason for a very high demand for it (annual production over 1.5 million tons[44]). Despite being crucial for market, nitriles can exhibit high toxicity,[46–48] and adiponitrile can pose a risk for human health (hence being listed in the List of Extremely Hazardous Substances by the US Environmental Protection Agency), especially at high concentrations.[49–51] The studies conducted on fish revealed the lethal concentration of AN LC_{50} between 670 and 2140 mg l^{-1} (ref. 50) (corresponding to 6.2 to 19.8 mM; the values are dependent on the species and the exposure duration), therefore, making it crucial to introduce a reliable method of monitoring adiponitrile levels in the environment.

Pillar[*n*]arenes are a comparatively new and highly versatile class of macrocycles constructed by hydroquinone unites para-bridged with methylene groups.[52,53] The smallest and the most extensively investigated macrocycle among pillar[*n*]arenes is pillar[5]arene, which is characterized by pronounced affinity towards various types of molecules, including positively charged and neutral species[54–57] such as triazoles, imidazoles,[58,59] and pyridine[60] derivatives. An especially high affinity is demonstrated in the complexation with various nitriles.[51,61] Due to its unique complexation properties and a vast variety of possible property tuning ways *via* rim group modification[62,63] pillar[5]arene has found broad application as adsorbent,[51] molecular sensor[64–68] and as a building block for the construction of supramolecular responsive materials.[69–74]

In the current work, we aimed at designing a supramolecular sensor chip for the detection of adiponitrile. Benefiting from a stable complex formation between pillar[5]arenes and adiponitrile, a gel-based sensor was developed bearing two types of crosslinks: chemical (irreversible) and supramolecular (labile), the latter based on a host–guest complex with pillar[5]arene. Upon the presence of the analyte in the medium around a pre-swollen gel, the competitive complexation takes place with the analyte displacing the original guest species, which leads to disruption of the crosslinks and, thus, to the decrease in the crosslink density. This change can be measured by change in the swelling using a sensitive SPR technique (Fig. 1).

Results and discussion

Synthesis and general considerations

Synthetic strategy. For a fabrication of a dually crosslinked system, it can be very beneficial to obtain separately host and guest polymers (*i.e.*, polymers with pendant host and guest groups) which upon mixing would produce a supramolecular gel. Introduction of a photo-crosslinking moiety, such as dimethylmaleimide,[40,75–79] brings an advantage of on-demand permanent crosslink formation, which can be used to form a chemical gel in any form upon irradiation with light after conveniently processing the polymer blend as a solution. Such host, guest and crosslinker groups can be embedded into polymer chains either as comonomers in a copolymerization process or in course of post-modification of polymers containing reactive groups. The former approach is not free from disadvantages: firstly, the monomers might not have similar reactivities, thus, leading to an uneven distribution of functional groups along the chain; secondly, this approach is less flexible towards the composition of the resulting copolymers. Therefore, we chose the post-modification approach, since it requires less components for the polymerization step (which means a higher adjustability), and the initial polymer can be used for both host and guest polymers implying a similar distribution of pendant moieties. As mentioned above, such post-modification requires a presence of a reactive comonomer, such as 4,4-dimethyl-2-vinylazlactone (VDMA).[80,81] VDMA has been gaining an increasing attention as a comonomer possessing an electrophilic ring, which can be opened in a "click"-manner at a high rate and efficiency by various nucleophiles, especially by amines.[82–84] Recently, the advantages of this versatile monomer were employed to create adjustable and smart co- and block-copolymers.[79,85–89] Hence, the utilization of a

copolymer containing VDMA allows highly efficient post-modification by a species possessing an amine functionality, which serves as a foundation for the design of host and guest moieties.

One of the features of pillar[*n*]arenes that make them highly versatile host species is the possibility of their functionalization *via* rim-group substitution.[53,63] Hence, various strategies were developed which paved the way for selective substitution of one, two or more alkyl rim groups as well as for achieving regioselectivity thereof.[63,90,91] For a fabrication of host polymers with pendant P5A groups a selective mono-substitution is required, which can be implemented by two major approaches: (1) by co-cyclooligomerization (the functionality is introduced directly during the macrocycle formation) and (2) by forming "homo"-P5A followed by mono-demethylation and subsequent etherification. We chose the second pathway (Fig. 2A) for several reasons. P5A in the first step can be produced in a relatively high yield (>70%) and on a gram scale without complex purification. For the selective mono-demethylation using BBr_3 it is crucial to find the perfect conditions, however, the unreacted P5A can be recovered from the mixture, which minimizes losses and makes this procedure effective considering the overall yield. P5AOH containing a single hydroxyl group can be easily converted into a mono-functionalized P5A, for instance, by Williamson etherification. In the current work, we sought to improve the versatility of this method by introducing a propargyl function as a side chain. This allows utilizing azide–alkyne [2 + 3]-cycloaddition for further functionalization. As a result, P5A with a single triazole-containing amine-terminated side chain (HT) was synthesized with a yield of 17% over 5 steps. The characterization of the obtained products can be found in the ESI (Fig. S1–S4 and S9–S18†).

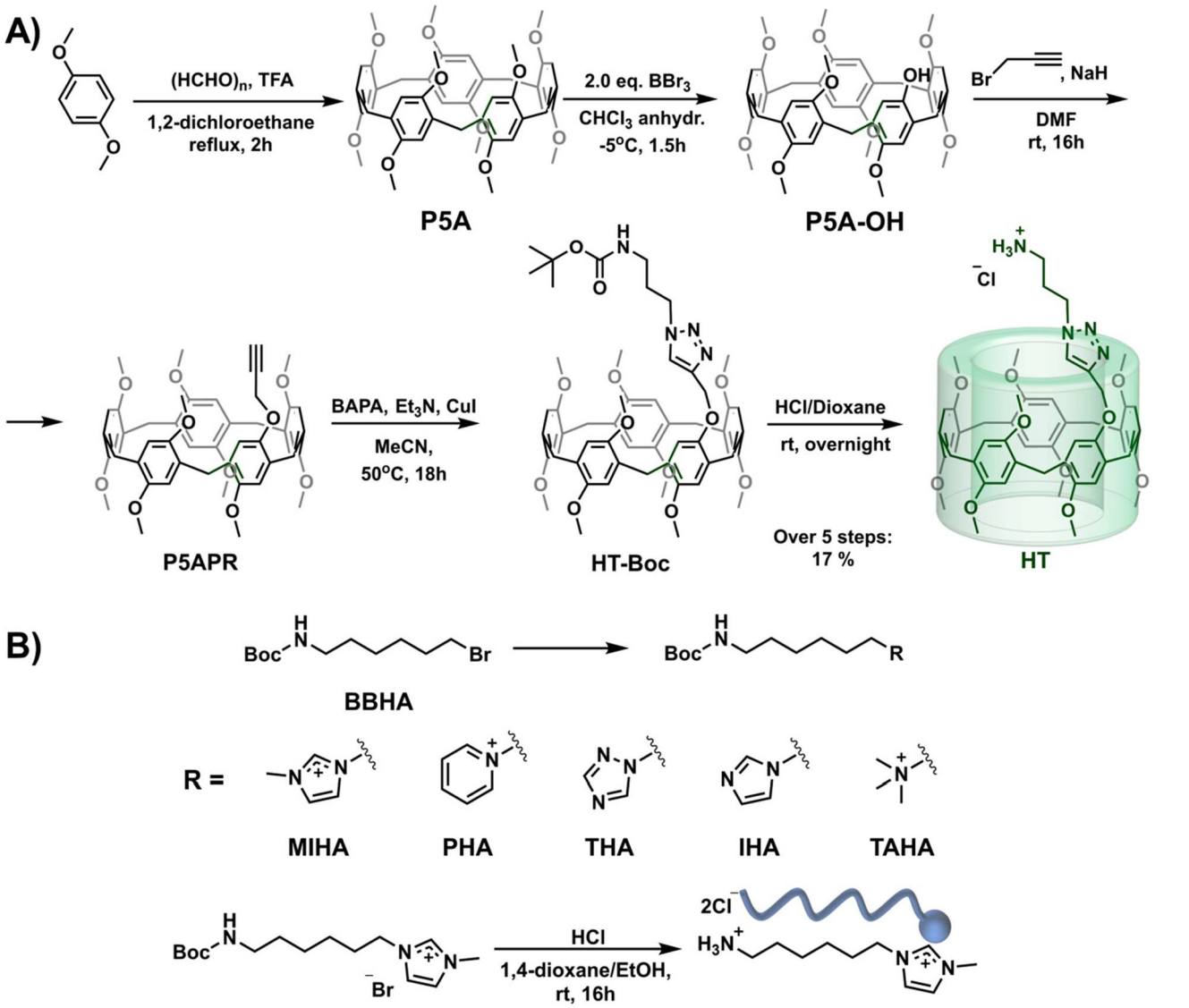

Fig. 2 Synthetic routes towards (A) host moiety (HT) and (B) guest moieties (MIHA, PHA-Boc, THA-Boc, IHA-Boc and TAHA-Boc). For the detailed synthetic procedures see experimental part and ESI.†

Choice of a solvent. For the binding studies as well as for AN detection using the gel sensor chloroform was selected as a solvent for several reasons. Firstly, solubility of the investigated host and guest species is high enough for performing NMR titration experiments in this solvent. Secondly, the combination of relative low polarity as well as bulkiness of $CHCl_3$ stimulates the binding between P5A and guests in comparison to high-polarity solvents (such as acetone or DMSO) or solvents that act as guest species themselves (for instance, CH_3CN or acetone).[92] High binding affinity is, in its turn, beneficial for both stability of the second crosslink in the gel and its sensitivity upon presence of the analyte. Thirdly, the fabricated polymers (as discussed further) were as well soluble in chloroform, therefore, providing an adequate estimation of the system behaviour already on the low-molecular stage of investigations.

P5A-AN complexation. In order to create a chemoresponsive gel with supramolecular crosslinks which would break upon the presence of the analyte, a thorough selection of a host–guest system is required. The complex should possess a binding affinity in a certain range. On the one hand, it should not exceed (actually, be at least one order of magnitude lower) the affinity between the analyte and the host moiety, otherwise the analyte in the solution would not have any effect on the crosslink density and, therefore, on the swelling behavior. On the other hand, if the binding affinity is too low, the crosslinking might not be formed at all, which, again, means a drastic decrease in responsiveness. As shown by Shu *et al.*,[61] adiponitrile (AN) is capable of forming particularly stable pseudorataxanes with pillar[5]arenes due to the combination of C–H···π and dipole–dipole interactions. In the paper, the authors were unable to deliver any value for K_a for the system per-*O*-alkyl-P5A/AN in $CDCl_3$ because of the limitations of the NMR titration technique.[93–95] A similar trend is observed in the case of the AN@P5A complex. The NMR titration was conducted in $CDCl_3$ at the constant host concentration $[H]_0$ = 6 mM (Fig. S31 and S32†) and the results are in accordance with previously reported ones.[61] In the spectra peaks of both complexed and uncomplexed species are observable indicating a slow exchange. Noticeably, the peaks of the free AN do not appear until the 1 : 1 host : guest ratio is reached, and upon further addition of the guest species the complete disappearance of the free host peaks was observed (Fig. S33†). All these facts speak in favor of a highly stable binding between both species.

Further details of the complexation equilibrium can be provided by 2D NOESY NMR (Fig. S34†). Notably, the strong negative cross-peaks demonstrate that the peaks of both free and "threaded" AN belong to the same molecule, which implies that although the pseudorotaxane exhibits slow equilibrium, the guest molecules still exchange in a cavity within the time of an experiment. This is further proved by NOE cross-peaks (marked green) which appear for all AN protons.

To have an insight into the complexation strength the titration curves were simulated using HySS 2009 (Version 4.0.31) software[96] for a two-component system of 1 : 1 stoichiometry and two different binding constants. The resulting curves (Fig. S35†; solid lines: $\log K_a$ = 5.0; dashed lines: $\log K_a$ = 4.0) resemble the evolution of free host [P5A], free guest [AN] and complex [AN@P5A] concentrations depending on the total guest concentration $[AN]_0$. As can be seen from the figure, for both K_a values the curves align almost perfectly with the experimental data (the discrepancies taking place because of the AN and AN@P5A peak broadening, which results in an addition integration error) and with each other, therefore, demonstrating that $\log K_a$ (AN@P5A) is exceeding 4.0 but cannot be precisely determined using NMR titration.

Candidates for a guest moiety. From these considerations, as well as taking into account possible sensitivity issues, the upper limit for the binding affinity of the desired guest moiety to P5A can be set at around $\log K_a$ = 3.5. It is known that pillar[5]arenes can form stable pseudorataxanes with various heterocycle-capped axles.[58] Noticeably high binding constant was reported for butanes capped with imidazol-1-yl ($\log K_a$ = 4.3), 1,2,3-triazol-1-yl ($\log K_a$ = 4.2) substituents for per-*O*-ethyl-P5A. For P5A the only reported value considers 1,4-bis(1,2,4-triazol-1-yl)butane ($\log K_a$ = 3.1) as a guest species. Besides, due to the electron-rich cavity of pillar[*n*]arenes and, therefore, possibility of exhibiting Coulomb interactions positively charged species can benefit from the complex formation compared to neutral molecules. D'Anna *et al.*[59] studied the effect of solvent and counterion on the stability of complexes of P5A with anthracenyl substituted alkylimidazolium species by UV/Vis spectroscopy. According to their report, the K_a varied between 10^3–10^4 M^{-1} for all the investigated solvents (2300 M^{-1} in case of chloroform) except DMF where the stability was significantly lower. Besides, the complex with Cl^- anion is shown to exhibit especially high stability compared to complexes with other counterions (K_a = 4700 M^{-1}). Bis(imidazolium) substituted butanes were investigated for their interaction with per-hydroxy-P5A[97] in DMSO, acetone, their mixtures and a mixture of acetone and chloroform (1 : 1). It was found that the binding affinity increases with increasing acetone : DMSO ratio (from $\log K_a$ = 1.74 for pure DMSO up to 2.66 for acetone) and became even stronger in acetone : chloroform mixture ($\log K_a$ = 3.49). Similar trend was observed for bis(methylimidazolium)butane with $\log K_a$ reaching 3.00 for acetone : DMSO (3 : 2). In a solvent mixture with chloroform the complex was insoluble. The same group studied complexation between the same macrocycle and a broad range of paraquats and bis(pyridinium) derivatives in DMSO.[60] It was found that the bis(pyridinium)alkanes have a higher binding affinity (up to $\log K_a$ = 2.65 for bis(pyridinium)butane) towards per-hydroxy-P5A in DMSO than paraquats. Furthermore, methylimidazolium[98] and pyridinium[70,71,99] derivatives have been successfully used by various working groups as guest moieties for the preparation of pillar[*n*]arene-based gels. Final condition, since the host and guest moieties are designed as pendant groups on the polymer chains, the desired axles should only have one side substituted.

In this work, with regard to the polymer post-modification arrangement, 6-aminohexan-1-ol was chosen as a basic building block for the guest moieties. After substitution of OH group with a bromine by refluxing in a concentrated HBr and

subsequent Boc-protection, it was reacted with various nitrogen-containing species to obtain corresponding guests (Fig. 2B, S5–S8 and S19–S30†). We chose the following axle substituents as potential candidates for the role of the guest in the gel sensor: imidazol-1-yl, (3-methyl)imidazol-1-yl, 1,2,4-triazol-1-yl, pyridinium and trimethylaminium moieties.

NMR investigations of host–guest interactions

NMR titration studies. In order to choose the best candidate, NMR titrations were conducted using Boc-protected aminohexane bearing the corresponding groups on the other end of the alkyl chain: IHA-Boc, MIHA-Boc, THA-Boc, PHA-Boc and TAHA-Boc (Fig. 2B). Boc-protected moieties are much closer chemically to the pendant group structure in real gels (compared to the deprotected ones which are required for polymer modification), hence they were selected for the NMR titration. From the investigated guest moieties, MIHA-Boc (Fig. 3 and S36†), PHA-Boc (Fig. S39–S41†) and THA-Boc (Fig. S45–S47†) exhibited fast exchange, while IHA-Boc (Fig. S50–S52†) and TAHA-Boc (S54–S56†) showed slow exchange on the NMR time scale, which is indicated by the presence of separate peaks of free and complexed species. For each complex Guest@P5A the titration was conducted up to 3.25–4.7 guest moiety equivalents. In case of the fast-exchange systems, the assignment of the proton signals of complexes was conducted by the analysis of the corresponding peak shifts evolution in the NMR titra-

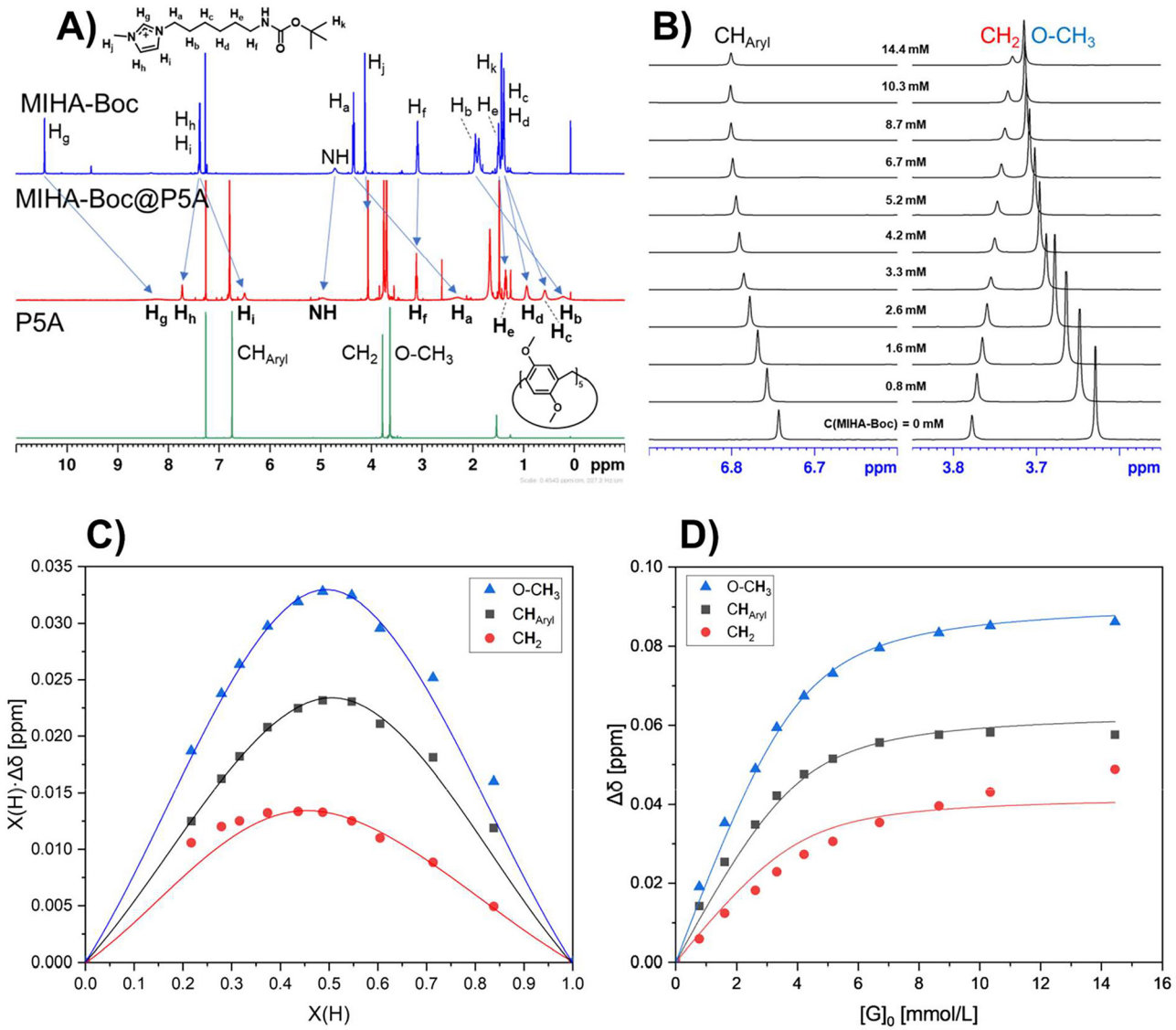

Fig. 3 (A) NMR spectra of (from the bottom) P5A, MIHA-Boc@P5A complex (at $[G]_0$ = 3.3 mM), MIHA-Boc. The change in peak shifts of the guest molecule is presented by the arrows. (B) Fragments of the NMR titration (MIHA-Boc@P5A), with shifts of only P5A peaks shown. (C) Job plot of the P5A-MIHA-Boc titration. The maximum of all three peaks of P5A lie around 0.5, which proves a 1 : 1 stoichiometry of the complex (the lines serve as guides for the eye). (D) Titration curves corresponding to the P5A protons. The fit curves are obtained using a non-linear least square method with K_a as a common parameter for all dependencies.

tion spectra as well as using 2D COSY NMR (Fig. S38 and S44†). For the systems exhibiting slow exchange, 2D NOESY spectra were analyzed to assign the signals (Fig. S53 and S58†).

The results of the NMR titration for the system P5A-MIHA-Boc is shown in Fig. 3 and S36.† In the spectra the shift of the peak positions can be traced. Firstly, the protons of the MIHA-Boc alkyl chain undergo an upfield shift, which is induced by the inclusion of the guest molecule into the macrocycle. It can be noticed that the closer a methylene group is located to the imidazole fragment, the more pronounced the shielding effect is (Fig. 3A): whereas for the proton H_a (for $[H]_0:[G]_0 = 1:0.83$) the $\Delta\delta = -2.26$ ppm and a strong broadening is observed, for the proton H_e $\Delta\delta = -0.14$ ppm, and for H_f even a slight deshielding takes place: $\Delta\delta = +0.04$ ppm with almost no broadening of the signal. Similar trend (upfield shift and broadening of the alkyl chain signals) is observed for alkyl chains of other guest molecules: PHA-Boc, IHA-Boc and TAHA-Boc (Fig. S39, S40, S50, S51, and S54, S55†); in case of THA-Boc the formation of THA-Boc@P5A can be demonstrated[100] by broadening but no significant shift of the protons of the guest moiety is observed (Fig. S45 and S46†).

The protons of the functional end group, however, exhibit different trends. For MIHA-Boc, H_g which is normally the most deshielded due to the positive charge of the MIHA-Boc shows a very strong upfield shift and signal broadening in the presence of P5A ($\Delta\delta = -2.47$ ppm). The proton H_h, however, demonstrates an opposing trend with a downfield shift: $\Delta\delta = +0.40$ ppm.

As for P5A signals (Fig. 3B, S41, and S47†), a clear trend can be noticed that deshielding takes place for methoxy groups and aromatic protons, which is in accordance with earlier literature reports for P5A.[101] Interestingly, the protons of methylene bridges exhibit slight shielding in all fast exchange systems.

Further proof of pseudorotaxane formation can be delivered by 2D NOESY NMR. The presence of NOE cross-peaks between host and guest protons was observed in spectra of PHA-Boc@P5A and THA-Boc@P5A complexes (Fig. S43 and S49†). Surprisingly, the intensity of the NOE signals in case of MIHA-Boc@P5A was too weak (Fig. S37†).

The host peaks can be used to determine the stoichiometry of the Guest@P5A complexes and their binding constants. Job plots obtained from the shifts of each of the protons (Fig. 3C, S42A, and S48A†) indicate a 1 : 1 stoichiometry of the investigated pseudorataxanes MIHA-Boc@P5A, PHA-Boc@P5A and THA-Boc@P5A due to the maximum of all the curves lying at approx. 0.5. Using the non-linear regression method for the 1 : 1 complexation model (Fig. 3D, S42B, and S48B†), the constant K_a as a global parameter and the chemical shift at full complexation $\Delta\delta_{max}$ for each of the peaks were obtained (Table S1† and Fig. 4). It can be observed that from the systems with fast exchange on the NMR timescale the charged species (MIHA-Boc and PHA-Boc) have a significantly (by one order of magnitude) higher binding affinity (and therefore, more stable complexes) than neutral THA-Boc: $\log K_a = 3.32 \pm 0.10$, 3.66 ± 0.09 and 2.27 ± 0.04, respectively. The absence of

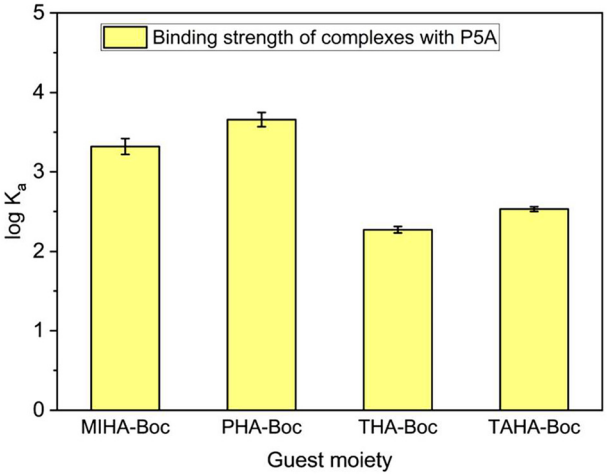

Fig. 4 Comparison of the binding affinities of P5A with different guests, as obtained in this work.

THA-Boc signal shifts can be hence explained by too weak interactions between the guest and P5A in $CDCl_3$.

As mentioned before, the results of this work suggest that the complexes IHA-Boc and TAHA-Boc exhibit slow exchange on the NMR timescale. For the IHA-Boc@P5A this finding correlates with an extensive studies of P5A complexes with imidazole-substituted alkanes performed by Li *et al.*[101] The protons of the end groups are in both complexes shifted upfield and broadened, and their proximity to the macrocycle protons is additionally confirmed by 2D NOESY for TAHA-Boc@P5A (Fig. S58†). Unfortunately, it was not possible to determine the same for the IHA-Boc@P5A complex (Fig. S53†) because of strong overlapping of signals.

The stoichiometry of the TAHA-Boc@P5A pseudorotaxane was determined by the peak integration to be 1 : 1 (host : guest), and the binding constant was calculated from the 1 : 1 mixture to be $\log K_a = 2.53 \pm 0.03$ (Fig. 4). The titration curves simulated for a system with $\log K_a = 2.53$ align well with the experimental data for the beginning of the titration, as shown in Fig. S57.†

Peak integration of bound P5A and IHA-Boc interestingly revealed a 1 : 2 (P5A : IHA-Boc) geometry for the whole range of titration ratios. The complexation constant K_a was calculated using the following equation from the spectrum of 1 : 2 (host : guest) mixture:

$$K_a = \frac{[HG_2]}{[H][G]^2} = 7900\ M^{-2}$$

where $[HG_2]$ is the concentration of the complex $(IHA\text{-}Boc)_2$@P5A, [H] and [G] are the concentrations of free P5A and IHA-Boc, respectively.

The detailed discussion of the NMR-titration of P5A with PHA-Boc, THA-Boc, IHA-Boc and TAHA-Boc can be found in ESI.†

DOSY NMR. A further insight into the complex formation between P5A and the guest moieties was provided by the

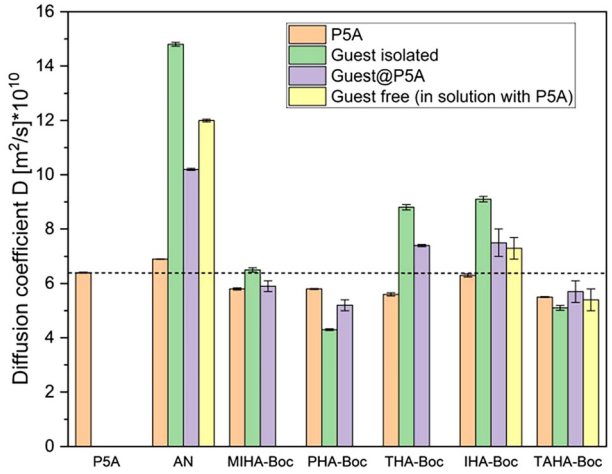

Fig. 5 Diffusion coefficients D for P5A and the discussed guest molecules alone and as parts of the host–guest inclusion complexes. In case of the complexes with a slow exchange, peaks of free and complexed species were evaluated separately. The dashed line represents a D value for P5A ($D = 6.4 \times 10^{-10}$ m^2 s^{-1}).

diffusion-ordered NMR in $CDCl_3$ (Fig. 5). Since P5A is a large molecule, its diffusion coefficient D can be expected to be lower than that of smaller and, hence, intuitively more mobile guest molecules. Moreover, after the formation of the inclusion complex, the coefficient D should become comparable to D_{P5A} because the dimensions of the pseudorotaxane are mostly determined by the dimensions of P5A if the guest moiety is fully encompassed by the host.[97] The graph in Fig. 5 demonstrates the clear difference between neutral and positively charged guest molecules: the former have higher D values than the latter roughly divided by the coefficient value of the P5A ($D_{P5A} = 6.4 \times 10^{-10}$ m^2 s^{-1}), the reason being arguably the solvation that occurs because of the polarity of the chloroform, which increases the size of the molecule in the solution, thus, hindering the mobility.

Being the smallest molecule among the investigated species, AN has by far the highest diffusion coefficient ($D_{AN} = 1.48 \times 10^{-9}$ m^2 s^{-1}). Upon presence of P5A the D_{AN} value drops down to 1.02×10^{-9} m^2 s^{-1} for the peaks of the "threaded" AN and to 1.20×10^{-9} m^2 s^{-1} if calculated for the peaks of "free" AN. This highlights the finding made with NOESY NMR that although the interaction is considered "slow" on the NMR timescale, the two states are not fully separated. Therefore, the diffusion coefficients of both free and complexed AN in solution are average values between the isolated and fully threaded AN. It is worth noting that due to the strength of the binding affinity of AN@P5A these two states are distinguishable, which is not the case for other guest species as will be shown further. Moreover, AN@P5A is the only pseudorotaxane by which the mobility of P5A slightly increases up to 6.9×10^{-10} m^2 s^{-1}.

Other guest molecules are larger in size and, therefore, possess smaller D values than AN. The diffusion coefficients of neutral THA-Boc ($D_{THA\text{-}Boc} = 8.8 \times 10^{-10}$ m^2 s^{-1}) and IHA-Boc ($D_{IHA\text{-}Boc} = 9.1 \times 10^{-10}$ m^2 s^{-1}) decrease upon presence of P5A in the system. The value of $D_{THA\text{-}Boc@P5A} = 7.4 \times 10^{-10}$ m^2 s^{-1} as expected for a fast exchange complex, lies as an average between pure guest and pure host. P5A diffusion is noticeably hindered as well, which implies a size increase of the macrocycle upon threading with THA-Boc. The same behavior is observed in case of the pseudorotaxane IHA-Boc@P5A, where the differences in mobility between "free" and complexed guest molecules is within the error and, therefore, insignificant ($D_{IHA\text{-}Boc@P5A} \approx 7.4 \times 10^{-10}$ m^2 s^{-1}). The diffusion coefficients of the isolated charged guests are comparable to ($D_{MIHA\text{-}Boc} = 6.5 \times 10^{-10}$ m^2 s^{-1}) or lower than that of P5A ($D_{PHA\text{-}Boc} = 4.3 \times 10^{-10}$ m^2 s^{-1}, $D_{TAHA\text{-}Boc} = 5.1 \times 10^{-10}$ m^2 s^{-1}). As was with THA-Boc@P5A, for the complexes exhibiting fast exchange the D value resembles an average between D values for host and guest (for MIHA-Boc the values are within an error from each other). In case of TAHA-Boc@P5A because the diffusion coefficient of the isolated guest ($D_{TAHA\text{-}Boc} = 5.1 \times 10^{-10}$ m^2 s^{-1}) is close to the D of the complexed P5A, the values of the complexed TAHA-Boc do not change much upon presence of the host species.

Hence, using DOSY NMR it could be demonstrated that the formation of the host–guest assemblies studied in the current work is affecting their mobility and size. Furthermore, alteration of the mobility upon complexation was found to follow the pattern of fast exchange complexes, *i.e.*, where the resulting diffusion coefficient of the guest was an average value rather than completely reduced to the mobility of P5A, which is in agreement with the previously discussed NOESY results.

Guest moiety selection. From the investigated guest moieties two candidates – MIHA and PHA – demonstrated the highest binding affinity towards P5A. Despite the K_a of the complex MIHA-Boc@P5A being lower than that of PHA-Boc@P5A, they are of the same order of magnitude, and both moieties were used to construct supramolecular gel systems by various research groups.[70,71,98,99] Nonetheless, lower binding affinity means a slightly higher lability in the presence of competitive guests, therefore, a higher sensitivity towards AN, which is beneficial for the fabrication of a sensor with a detection mechanism based on competitive complexation. Based on this, we have selected MIHA as a guest moiety for further fabrication of a guest polymer.

Polymer synthesis and modification

VDMA as "click"-modifiable monomer was synthesized in two steps form 2-methyl alanine by a slightly modified procedure from ref. 87. DMIEA was obtained according to a known literature procedure.[40] Since DMIEA contains a 3,4-maleimide fragment, as mentioned above, it is capable of UV-light-induced [2 + 2]-dimerization for the subsequent gelation of the polymer blends.

VDMA was copolymerized with dimethyl acrylamide (DMAAm; DMAAm to VDMA ratio 80 : 20) using RAFT polymerization with DMP as chain transfer agent and AIBN as initiator (Fig. 6 and S59†). Controlled radical polymerization was selected for achieving a regular distribution of monomers in the copolymer (however, VDMA is known to have a higher

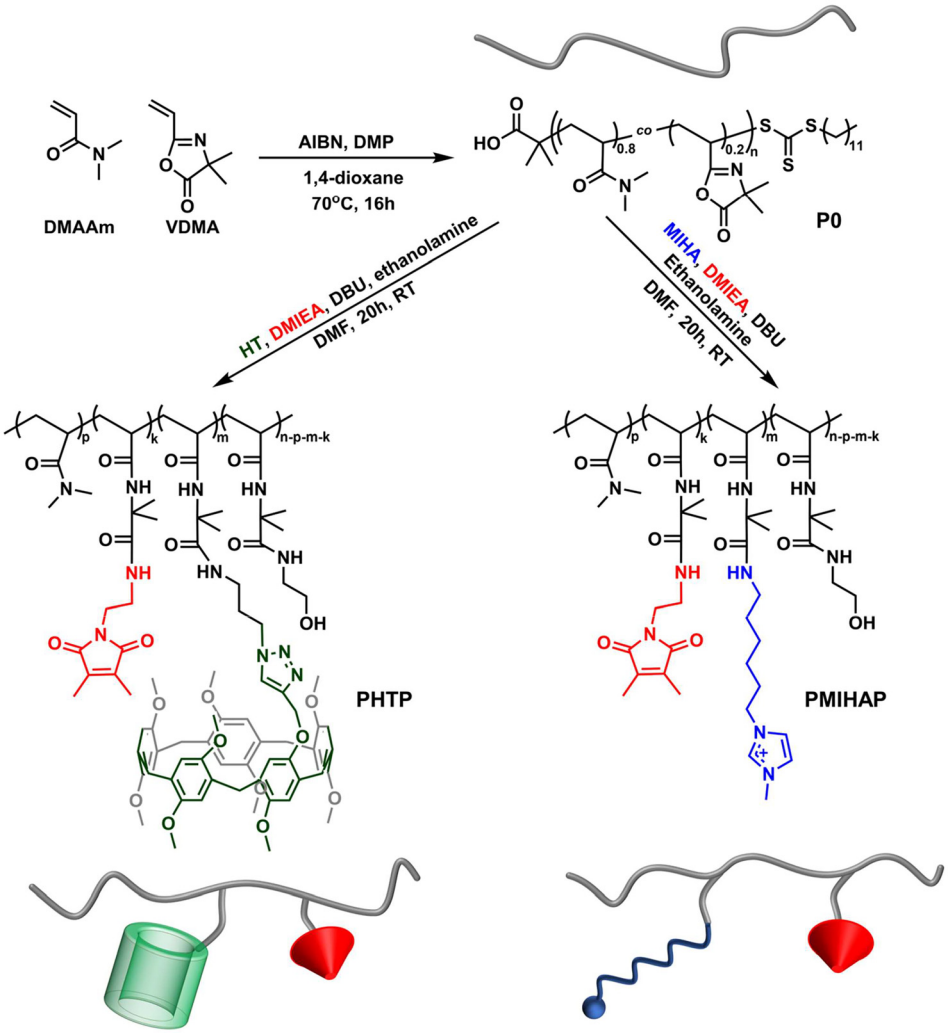

Fig. 6 RAFT polymerization of VDMA and DMAAm to a copolymer P0 and polymer modification using host and guest moieties as well as photo-crosslinker. For the detailed synthetic procedures see experimental part and ESI.†

copolymerization rate than DMAAm[79]). The molecular weight (M_n) of p(DMAAm-*co*-VDMA) copolymer (P0) is presented in the Table 1 and Fig. S63.† Because of the susceptibility of VDMA groups towards hydrolysis, the fresh copolymer was stored under inert atmosphere in a tightly closed vial in a freezer.

Table 1 Properties of the obtained polymers

Polymer	Functionality	Host or guest group,[a] %	Photo-cross-linker,[a] %	M_n [b]	$Đ$[b]
P0	—	—	—	53 400	1.90
PHTP	HT, DMIEA	11%	2.8%	103 200	2.21
PMIHAP	MIHA, DMIEA	12%	2.8%	68 900	2.57
PPC	DMIEA	—	16%	92 700	4.45

[a] Determined by ^{1}H NMR spectroscopy. Per cent of total number of monomer units. [b] Determined by size-exclusion chromatography.

P0 was used for further post-modification to obtain a host polymer (PHTP, containing HT and DMIEA as pendant groups, Fig. S60†), a guest polymer (PMIHAP, containing MIHA and DMIEA, Fig. S61†), and a photo-crosslinker-modified polymer (PPC, containing only DMIEA groups, Fig. S62†). All moieties (HT, MIHA and DMIEA) were attached to the polymer chains by mixing them with P0 in DMF in the presence of DBU. Because VDMA undergoes the ring opening with nucleophiles, DBU was used to deprotonate the amine hydrochlorides thus increasing the nucleophilicity. By devising the modified polymer composition, the amount of the photo-crosslinker DMIEA was aimed at 3 mol% since it was demonstrated earlier in our working group that the DMIEA monomer ratio of as low as 2.3% allows a stable gel formation.[40] Furthermore, preliminary studies showed that at the host and guest modifier ratio of 5–6% the responsivity and sensitivity of the system towards

AN is insufficient, thus, their content was increased up to 11% and 12% for HT and MIHA, respectively. It is worth mentioning that all polymers including PHTP were water-soluble, therefore, it was possible to purify them by dialysis in water.

The effectiveness of the polymer modification, *i.e.*, the functional groups content in the resulting polymers was calculated (Table 1) by integration of the corresponding NMR signals. GPC results (Table 1 and Fig. S63†) demonstrate that upon modification the increase in M_n of the polymer is observed, which is almost double as high in the case of PHTP compared to P0. This is expected due to a high molecular mass of the attached pendant groups (HT). Noticeably, the M_n of PPC is also significantly higher than that of the unmodified polymer. This can be explained by DMIEA moieties dimerizing during the polymer work up or storing leading to the crosslink formation between chains. This possibility is supported by a remarkably increased polydispersity of the sample.

SPR studies: adiponitrile responsiveness

Although it would be beneficial for the environmental monitoring to be able to determine AN concentration directly from wastewater samples, we consider water to be a poor solvent for the sensing platform in its current design because of, on the one hand, its high polarity which leads to a highly energetic solvation of the charged MIHA pendant groups, thus, hampering the initial host–guest complex formation. On the other hand, considering an exceptional hydrophobicity of P5A groups, water as a solvent promotes their aggregation, which not only hinders the possibility of MIHA@P5A formation even further, but also it decreases the number of P5A units available for binding with AN. As discussed above, $CHCl_3$ was selected for the detection studies due to a good solubility of unmixed host and guest polymers as well as proven high binding affinities of the participating species, which implies a high sensitivity of the designed sensor.

The sensor chips prepared by dip-coating in an adhesion promoter solution,[102] followed by spin-coating, drying *in vacuo*, photo-crosslinking using UV irradiation and equilibration in $CHCl_3$ were investigated by surface plasmon resonance spectroscopy (Fig. 7). Here, the gel swelling behavior was studied in $CHCl_3$ and in the presence of the analyte – AN. The scan measurement of a golden layer and a dry gel are demonstrated on Fig. S64.† The plasmon resonance minimum is strongly shifted to higher angles ($\theta_{PR} \approx 90°$) indicating a high refractive index and, accordingly, high gel density. The parameters of the gel layer, obtained by a fit simulation are given in Table S2.† The fit is not matching the experimental SPR curve perfectly because of the inhomogeneities on the gel surface, however, it is possible to draw conclusions about the parameters of the gel by fitting the area around the angle of total internal reflection (20°–25°) and the plasmon resonance minimum.

Through the flow cell 1 ml $CHCl_3$ was pumped using a syringe and the gel was equilibrated for 2 h. Then, the gel layer was treated with AN solutions of increasing concentrations (in each case, 1 ml of the corresponding solution was injected into the flow cell and the gel was equilibrated for 10 min): 1 μM, 5 μM, 10 μM, 20 μM, 50 μM, 100 μM, 200 μM, 500 μM and 1 mM. Between every two injections the flow cell was purged with 1.5 ml $CHCl_3$. The gel behavior was investigated using kinetic measurement at 76°. As can be seen from Fig. 8 (A), the system PHTP + PMIHAP exhibits almost no responsiveness up to C_{AN} = 20 μM, followed by a decrease of intensity at a constant angle with an increasing concentration resulting in a linear dependence from log C_{AN}. It is worth noting that the system exhibits almost complete recovery of the intensity upon rinsing with $CHCl_3$, which proves the reusability of the constructed sensor chip.

To determine the sensitivity of the chip, scan measurements were performed after each AN solution injection and

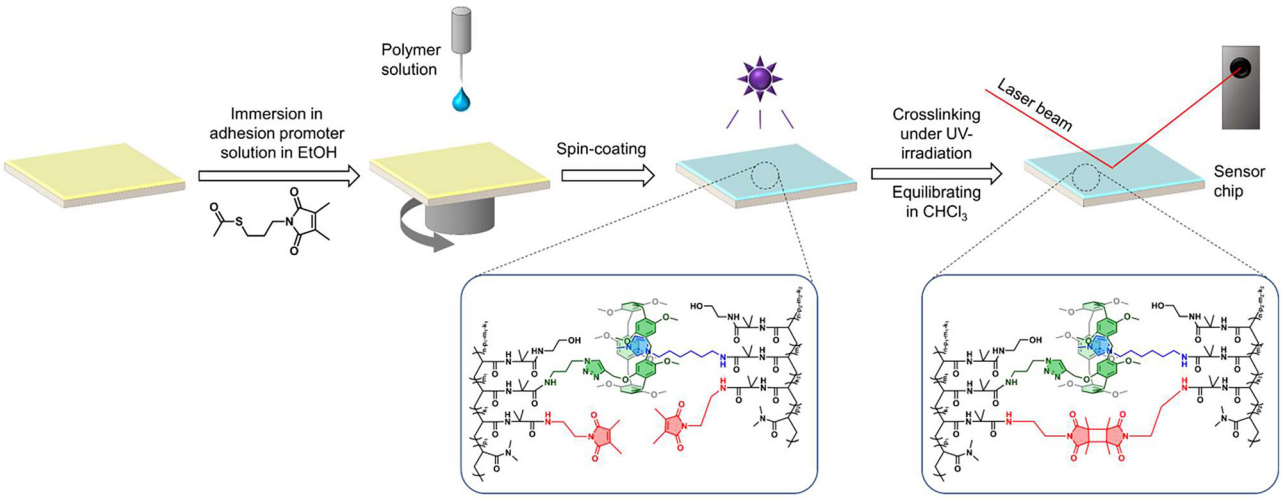

Fig. 7 SPR sample preparation. Gold-coated N-LaSF9 wafer is immersed in an adhesion promoter solution overnight. Then, a polymer (mixture) solution is spin-coated onto the wafer, followed by drying *in vacuo* and crosslinking by UV-irradiation. After equilibrating in $CHCl_3$ overnight the sensor chip can be measured.

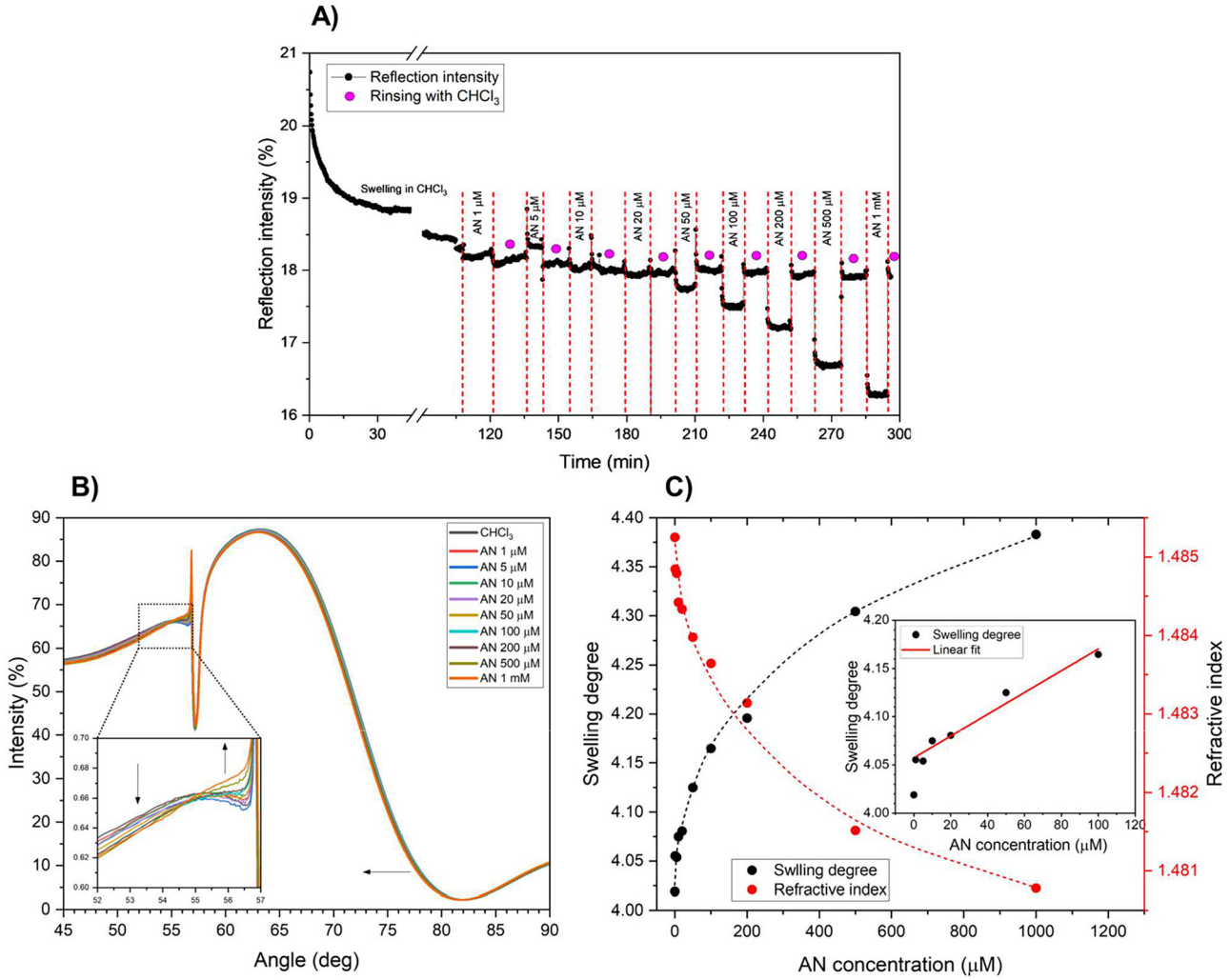

Fig. 8 SPR measurement of the PHTP + PMIHAP sensor chip with different concentrations of AN in $CHCl_3$. (A) Kinetic studies at 76°. Between swelling in AN solutions the gel was rinsed with $CHCl_3$, which led to the gel returning to its initial state. (B) SPR scan measurements of the gel swollen in AN solutions. (C) Dependence of swelling degree and refractive index with increasing AN concentration (dashed lines serve as guides for the eye). Inset: linear fit of the first section of the graph.

equilibration. The angular spectra of the swollen gels are presented on Fig. 8(B). In the spectra two features are clearly recognizable and the changes in the system affect these regions the most: the plasmon resonance around 82° and the waveguide (56°–58°). For layers of high thickness (>300 nm) in a one-layer model the former is affected by the refractive index n_d, whereas the latter by both the refractive index and the layer thickness.[103] The shift of the plasmon minimum to the lower angles observed in Fig. 8(B) implies a decrease in n_d is and, therefore, evidence of the decreasing gel density upon the addition of AN, which is expected due to the crosslinks being broken because of the competitive complex formation. Simultaneously, the change in the waveguide region can be noted, serving as a hint about gel thickness changes. For the determination of the gel layer thickness the curve simulation based on Fresnel equations is required. Unfortunately, for the obtained spectra, the one-layer model failed to deliver a precise curve fit. Thus, a two-model simulation was utilized, which considers the anisotropic character of the gel swelling.[102,103] In this model, the parameters of the inner layer affect the plasmon minimum region the most, and the waveguide region can be precisely fitted by optimizing the parameters of the outer layer.

From the Fig. 8(C) and Table S2† it is clear that the sensor chip developed in this work shows responsiveness towards adiponitrile. With an increasing concentration of the analyte the gel thickness d (and, therefore, swelling degree Q) increases and the refractive index decreases, indicative of a reduced density likely caused by breaking of the supramolecular host–guest crosslinks through a competitive complex formation. It is worth noting that according to the obtained parameters the inner layer does not undergo significant changes upon increasing AN concentration with the layer thickness d^{in} staying between 262–273 nm, whereas the outer layer thickness d^{out}

increases from 483 up to 558 nm with a significant decrease in refractive index.

It can also be noticed in linear coordinates that saturation of the supramolecular system is occurring with increasing AN concentration. Thus, a linear section of the swelling degree dependence (Fig. 8, inset of C), was chosen for the determination of the limit of detection for the fabricated sensor chip (Table S4†):[104] LoD = 25 μM.

The achieved limit of detection is significantly lower than the concentration limit in the toxicity evaluation against fish as discussed earlier.[50] This proves that the sensitivity of the devised sensor chip is sufficient for the detection of AN concentrations that can pose a threat to the environment. Nevertheless, the value can be improved further, in our view, by optimizing the designed sensing platform on chemical and/or methodological levels for further fabrication of sensing devices.

To prove that the responsiveness of the gel sensor is based on the built-in host–guest interactions and to separately evaluate the influence of the other polymer components (DMIEA and DMAAm) on the interaction with AN, an SPR measurement was conducted using a wafer coated with PPC, *i.e.*, not containing any host or guest groups (Fig. S65†). The gel was measured in a dry state as well as swollen in $CHCl_3$ and in 1 mM AN solution (therefore, exposing it to a high concentration). Fig. S74† shows that no difference is noticeable between the two curves, and Table S3† reveals that upon presence of the analyte the PPC gel even exhibits a very slight shrinking, thus confirming the expected mechanism of AN interaction with PHTP + PMIHAP gel sensor.

Experimental section

Materials

N,*N*-Dimethyl acrylamide (TCI) was purified by vacuum distillation before use. The solvents: acetone, chloroform, dichloromethane (DCM), diethyl ether, ethyl acetate (EtOAc), isohexane and methanol (MeOH) were received from Stockmeier and purified by distillation before use. Deuterated solvents: $CDCl_3$ (99.8% D, with Ag), DMSO-d_6 (99.8% D), CD_3CN (99.0% D) and D_2O (99.9% D) were purchased from Deutero GmbH and used as received. All the other chemicals were purchased from the corresponding supplier as listed below and used without further purification.

1,2,4-1*H*-Triazole (98%, Janssen Chimica), 1,2-dichloroethane (DCE) (99.8%, Riedel-de Haën), 1,4-dimethoxybenzene (99+%, Acros Organics), 1,4-dioxane (99.5%, Grüssing GmbH), 1,8-diazabicyclo[5.4.0]undec-7-en (DBU) (98%, Sigma Aldrich), 1-methyl-1*H*-imidazole (99%, Sigma Aldrich), 2-(dodecylthiocarbonothioylthio)-2-methylpropionic acid (DMP) (98%, Sigma Aldrich), 2,3-dimethylmaleic anhydride (97%, Acros Organics), 2,6-di-*tert*-butyl-4-methylphenol (BHT) (99%, Fluka), 2-methyl alanine (98%, TCI), 3-bromopropylamine hydrobromide (98%, Sigma Aldrich), 6-aminohexan-1-ol (97%, Sigma Aldrich), acetonitrile (MeCN) (99%, Fisher Chemical), acryloyl chloride (97%, Sigma Aldrich), adiponitrile (AN) (98%, TCI), allyl amine (98+%, Alfa Aesar), azobis(isobutyronitril) (AIBN) (recrystallized from ethanol, Sigma Aldrich), boron tribromide (1 M in dichloromethane, Sigma Aldrich), copper iodide (99.999%, Sigma Aldrich), di-*tert*-butyl dicarbonate (Boc_2O) (97%, Thermo Fisher), ethanol (EtOH) (99.5%, Grüssing GmbH), ethanolamine (99%, Acros Organics), ethyl chloroformate (97%, Sigma Aldrich), ethylene diamine (EDA) (99%, Acros Organics), 1,1,1,3,3,3-hexafluoropropan-2-ol (HFIP) (99%, Carbolution), hydrogen bromide (48% in H_2O, Sigma Aldrich) hydrogen chloride (4 M solution in 1,4-dioxane, Thermo Fisher), hydrogen chloride (37% in H_2O, Stockmeier), imidazole (99%, Merck), magnesium sulfate (anhydrous, VWR), *N*,*N*-dimethyl formamide (anhydrous, 99.8%, Thermo Fisher), paraformaldehyde (95+%, Sigma Aldrich), potassium trifluoroacetate (CF_3COOK) (98%, Sigma Aldrich), propargyl bromide (80% in toluene, Alfa Aesar), pyridine (99.5%, Acros Organics), sodium azide (99%, Merck), sodium carbonate (anhydrous, VWR), sodium chloride (anhydrous, Stockmeier), sodium hydride (60% in mineral oil, Acros Organics), sodium hydroxide (anhydrous, Normapur), sodium sulfate (anhydrous, VWR), tetrahydrofuran (THF) (99.5%, Acros Organics), thioacetic acid (98%, Acros Organics), toluene (technical grade, Stockmeier), triethylamine (TEA) (99.5%, Sigma Aldrich), trifluoroacetic acid (TFA) (99%, Thermo Fisher), trimethylamine (33% in ethanol, Fluka).

Methods

Melting point. The determination of melting point was conducted using Büchi Melting Point B-545 apparatus at a heating rate of 1 °C min^{-1}.

Nuclear magnetic resonance spectroscopy (NMR). NMR spectra were recorded on a Bruker Avance 500 spectrometer (500 MHz for ^1H) and a Bruker Ascent 700 spectrometer (700 MHz for ^1H and 176 MHz for ^{13}C). Chemical shifts (δ) are listed in ppm (relative to the solvent peak) and coupling constants (J) in Hz. Spectra processing was conducted using Bruker TopSpin 4.1.1. software.

NMR titration was conducted in $CDCl_3$ as follows.[105] Into an NMR tube with 0.5 ml host solution (0.004 M) aliquots of host–guest solution (0.004 M host and 0.02 M guest) were successively added. The tube was gently shaken and sonicated for 5 min prior to each NMR measurement. Determination of binding constants K_a for complexes exhibiting a slow exchange proceeded using a single point method.[58,61,97,101,106–109] The stoichiometry was determined by the integration of NMR signals, and for 1 : 1 (host : guest) complexes the binding constant was calculated from the equilibrium:

$$K_a = \frac{[HG]}{[H] \cdot [G]}$$

where K_a is a binding constant, [H], [G] and [HG] are equilibrium concentrations of host, guest and complex species. After obtaining titration curve the data was compared to titration curves simulated for a 1 : 1 complex using HySS 2009 (Version

4.0.31) software.[96] For the simulation the K_a value obtained experimentally was used.

In case of the fast exchange complexes for the determination of the stoichiometry of a complex a Job plot was used. The shift of host peaks was monitored, and the titration curves were fitted using the equation:[93,94]

$$\Delta\delta = \frac{\delta_{HG}}{2 \cdot [H]_0}\left(\left([G]_0 + [H]_0 + \frac{1}{K_a}\right) - \sqrt{\left([G]_0 + [H]_0 + \frac{1}{K_a}\right)^2 - 4 \cdot [H]_0 \cdot [G]_0}\right)$$

where $\Delta\delta$ is the host peak chemical shift, δ_{HG} is a theoretical chemical shift at the infinitely large guest concentration, $[H]_0$ is the total host concentration, $[G]_0$ is the total guest concentration. K_a is the binding constant. For each complex the titration curves of all three pillar[5]arene signals were fitted using a general fit with the same parameter K_a.

Mass spectrometry (MS). High-resolution mass spectra were recorded using Synapt-G2 HDMS mass spectrometer by Waters equipped with a quadrupole-time-of-flight detector. Electron spray ionization with following parameters was used as an ionization method:

Capillary voltage: 2.62 kV
Sample peak voltage: 10 kV
Extraction peak voltage: 3.2 kV

Size exclusion chromatography (SEC). For the determination of the molecular weight and molecular weight distribution HFIP + 0.05 M potassium trifluoroacetate was used as eluent with BHT as an internal standard at the flow rate of 1.000 ml min^{-1}. The system was equipped with a preliminary column (PSS-PFG guard 7 μm) and two consecutive columns (PSS-PFG 10^3 Å and 10^2 Å, 7 μm), a pump (Merck Hitachi L-6200) and an RI detector (Shodex RI 101). Samples were prepared with a concentration of 4 mg ml^{-1}. Molar masses were obtained according to the calibration using poly(methyl methacrylate) standards.

Surface plasmon resonance spectroscopy (SPR). SPR measurements were conducted in Kretschmann configuration using A RES-TEC RT2005 spectrometer from Res-Tec – Resonant Technologies GmbH. A monochromatic light from a He–Ne laser (λ = 632.8 nm) guided through a series of polarizers (Glan-Thompson polarizer, B. Halle) passed through a N-LaSF9 prism to reach the sensor chip. The reflected beam was further guided to a detector (a photodiode) coupled to a lock-in amplifier (7265 DSP, Signal Recovery). The sensor chip was attached to the prism using an index match (Cargille Lab., n_d = 1.8000 ± 0.005).[25] From the other side the chip was covered by a flow cell (*ca.* 1 cm^2) and the complete sample holder was mounted onto a goniometer (Huber Diffraktionstechnik GmbH & Co. KG) with sample and detector stepping motors (SLO-SYN® M061-LE02E by Superior Electric).

Kinetic measurements were performed at the fixed angle corresponding to approx. 30% signal intensity on the left slope of the plasmon minimum. The angular spectra were recorded as reflectivity *versus* angle $R(\theta)$ with θ ranging from 18° to 90°. The obtained spectra were fitted in Winspall software (MPI for polymer research, Mainz) using Fresnel equations to determine layer thicknesses (d) as well as refractive indexes (n_d) using a 2-layer model as follows:

The entire spectrum (45°–90°) was simulated and fitted iteratively by optimization of the x-minimum, *i.e.*, the plasmon resonance; only the parameters of the inner layer were varied during the iterative process. Further, d and ε_{real} of the inner layer were fixed for the second iterative process where parameters of the outer gel layer were varied. This was performed using the full curve optimization. The resulting layer thickness d was calculated as a sum of the thickness of both simulated layers, and the average refractive index n_{av} was obtained according to the following equation:

$$n_{D,av} = n_D^{out} \times \frac{d^{out}}{d^{out} + d^{in}} + n_D^{in} \times \frac{d^{in}}{d^{out} + d^{in}}$$

where n^{out} and d^{out} are the refractive index and thickness of the outer layer and n^{in} and d^{in} are the refractive index and thickness of the inner layer, correspondingly.

N-LaSF9 (n_d = 1.85025) glass wafers (25 × 25 × 1.5 mm) were purchased from ADVANCED OPTICAL COMPONENTS GmbH and coated with gold using PVD. Subsequently, the wafers were immersed in the adhesion promotor solution (1.2 mg ml^{-1} in EtOH) over night, rinsed with abs. EtOH and dried using a compressed nitrogen flow prior to applying a polymer layer (Fig. S57†).

Host and guest polymer solutions were prepared at a concentration of 4 wt% in DMF separately. After stirring both solutions for 1 h they were mixed at a 1 : 1 ratio of host and guest groups. The mixture was stirred overnight in a dark place followed by filtering through a Chromafil® PTFE syringe filter (0.45 μm) prior to spin-coating.

Spin-coating was carried out using a G3P-8 spin coater by Specialty Coating Systems. The polymer solution (*ca.* 80 μl) was applied onto the wafer by static dispense method and coated with a two-step program:

1200 rpm (20 s ramp) for 180 s;
1500 rpm (10 s ramp) for 60 s.

After the completion of the coating process the sample was dried *in vacuo* overnight in dark to remove the rest of the solvent.

Further, the polymer layer on the wafer was photo-crosslinked by UV-irradiation using an Omnicure S1500 UV lamp (250 mW cm^{-2}) for 300 s. The crosslinked gel layer was measured by SPR (dry layer thickness) after equilibrating in an anhydrous $CHCl_3$ overnight.

For the determination of the swollen gel layer thickness the chip was swollen in $CHCl_3$ in the spectrometer by pumping *ca.* 1 ml solvent through the cell and equilibrating for *ca.* 120 min before recording an angular spectrum. Then, for each swelling in AN solution, 1 ml was pumped through the cell and the system was equilibrated for 10 min before a scan measurement. Afterwards, the cell was purged with *ca.* 1.5 ml $CHCl_3$

the system was equilibrated for 10 min prior to injecting a further AN sample.

The limit of detection (LoD) was calculated by linear fit of the swelling degree dependence as a function of AN concentration according to the definition from:[104]

$$s_{y/x} = \sqrt{\left[\frac{\sum_i (Q_i - Q_{r,i})^2}{n-2}\right]}$$

$$\mathrm{LoD} = 3\frac{s_{y/x}}{A}$$

where Q_i–$Q_{r,i}$ is a difference between experimental and fitted value of swelling degree; n is the amount of data points; A is a slope of the linear fit.

Synthetic procedures

Synthesis of pillar[5]arene (P5A). The procedure was adapted from.[110]

Into a 500 ml 3-necked round-bottom flask 5.528 g (40 mmol) 1,4-dimethoxybenzene and 1.20 g (40 mmol) paraformaldehyde were suspended in 180 ml 1,2-dichloroethane followed by the addition of 20 ml trifluoroacetic acid. The reaction mixture was refluxed for 2 h. After cooling down the mixture was poured into 800 ml MeOH and the formed precipitate was separated using filter paper. Further, the crude product was resolved in 200 ml DCM and filtered through silica. After solvent evaporation the product was stirred in $CHCl_3$ for 30 min to remove the DCM molecules from the cavity. P5A (4.25 g; 5.7 mmol; 71%) was obtained as a white crystalline solid.

T_{mp} = 248.5–249.5 °C (Lit: 248.8 °C;[111] 248.1–249 °C[112]).

^{1}H NMR (700 MHz, $CDCl_3$) δ (ppm) = 6.83 (s, 10H, C**H**), 3.77 (s, 10H, C**H**$_2$), 3.70 (s, 30H, C**H**$_3$).

^{13}C NMR (176 MHz, $CDCl_3$) δ (ppm) = 150.8 (**C**$_{Ar}$–O), 128.4 (**C**$_{Ar}$–CH$_2$), 113.9 (**C**$_{Ar}$–H), 55.8 (**C**H$_3$), 29.6 (**C**H$_2$).

ESI-MS: cacld for $[M]^+$ m/z = 750.3404, found m/z = 750.3396.

Synthesis of monohydroxy-P5A (P5AOH).[113–115] In a dry 500 ml Schlenk flask under Ar atmosphere 3.2 g (4.26 mmol) P5A were dissolved in 200 ml $CHCl_3$ (preliminarily dried by distillation over P_2O_5), and the solution was cooled down to −5 °C on an ice/NaCl bath. After addition of 0.85 ml (8.5 mmol; 2 eq.) BBr_3 the flask was sealed with a septum and the mixture was stirred for 1.5 h. The reaction was quenched by pouring 100 ml H_2O into the mixture at vigorous stirring followed by neutralization by saturated Na_2CO_3 solution. The organic phase was separated, and the solvent was removed *in vacuo*. The crude product was purified by column chromatography (SiO_2; DCM : MeOH 100 : 0 to 100 : 1, R_f = 0.11). Since the monohydroxy- and dihydroxy-derivatives have similar retention factors,[115] for the isolation of the product the mixture was precipitated from 10 ml DCM solution into MeOH (40 ml) twice. Monohydroxy-pillar[5]arene (PA-OH) was obtained as white to slightly pink solid (0.8623 g; 1.17 mmol; 28%).

T_{mp} = 179 °C (Lit.: 203 °C[116]).

^{1}H NMR (700 MHz, $CDCl_3$) δ (ppm) = 6.88, 6.74, 6.71, 6.70, 6.66, 6.66 (s, 6H, C**H**); 6.63 (br s, 1H, O**H**); 6.62, 6.61, 6.59 (s, 3H, C**H**); 3.81 (s, 3H, C**H**$_3$); 3.78, 3.78, 3.78, 3.76 (s, 8H, C**H**$_2$); 3.74 (m, 5H, C**H**$_3$ and C**H**$_2$); 3.70, 3.63, 3.61, 3.61, 3.60, 3.57, 3.51 (s, 21H, C**H**$_3$).

^{13}C NMR (176 MHz, $CDCl_3$) δ (ppm) = 152.1, 151.3, 151.2, 151.2, 151.1, 151.1, 151.1, 151.0, 148.8, 147.8 (**C**$_{Ar}$–O); 130.2, 129.5, 128.9, 128.8, 128.5, 128.5, 128.3, 127.9, 127.0, 125.2 (**C**$_{Ar}$–CH$_2$); 119.1, 114.8, 114.8, 114.7, 114.5, 114.3, 114.3, 114.1, 113.2, 113.1 (**C**$_{Ar}$–H); 56.6, 56.6, 56.3, 56.3, 56.2, 56.1, 56.1, 56.0, 56.0 (**C**H$_3$); 31.2, 30.3, 30.1, 29.8, 29.1 (**C**H$_2$).

ESI-MS: cacld for $[M + Na]^+$ m/z = 759.3145, found m/z = 759.3137.

Synthesis of monopropargyloxy-P5A (P5APR). 0.86 g (1.17 mmol) P5A-OH were dissolved in 20 ml anhydrous DMF, and the solution was added at a vigorous stirring to a suspension of 95 mg (2.34 mmol; 2 eq.; 60% in mineral oil) NaH in 2 ml iso-hexane in a Schlenk tube under Ar flow. The mixture was diluted with DMF until cherry red color appeared. Then, 0.65 ml (80% toluene solution; 5.85 mmol; 5 eq.) propargyl bromide was added and the solution was stirred overnight at room temperature. After the reaction was complete, the mixture was poured into 200 ml DCM and washed with water (4 × 150 ml) to remove DMF. The organic phase was evaporated *in vacuo* and the crude product was purified by column chromatography (SiO_2; DCM 100%). Propargyl-P5A was obtained as a white to yellowish solid (0.8759 g; 1.13 mmol; 96%).

T_{mp} = 156.5–158.5 °C.

^{1}H NMR (700 MHz, $CDCl_3$) δ (ppm) = 6.79, 6.78, 6.78, 6.77, 6.76, 6.75, 6.75, 6.75, 6.74, 6.71 (s, 10H, C$_{Ar}$**H**); 4.40 (d, $^4J_{HH}$ = 2.36 Hz, 2H, O–C**H**$_2$); 3.79–3.76 (m, 10H, C$_{Ar}$–C**H**$_2$); 3.71, 3.67, 3.67, 3.66, 3.66, 3.6, 3.65, 3.63, 3.61 (s, 27H, C**H**$_3$); 1.82 (t, $^4J_{HH}$ = 2.02 Hz, 1H, C≡C**H**).

^{13}C NMR (176 MHz, $CDCl_3$) δ (ppm) = 151.5, 151.0, 151.0, 151.0, 151.0, 151.0, 151.0, 151.0, 150.9, 149.1 (**C**$_{Ar}$–O); 129.1, 128.7, 128.7, 128.6, 128.6, 128.5, 128.5, 128.4, 128.3, 128.1 (**C**$_{Ar}$–CH$_2$); 115.8, 114.6, 114.5, 114.4, 114.4, 114.3, 114.2, 114.2, 114.2, 114.1 (**C**$_{Ar}$–H); 78.9 (CH$_2$–**C**≡CH); 74.8 (C≡**C**H); 56.3 (O–**C**H$_2$); 56.1, 56.1, 56.1, 56.0, 56.0, 56.0, 56.0, 55.9, 55.9 (**C**H$_3$); 30.7, 30.0, 29.9, 29.9, 29.2 (C–**C**H$_2$–C).

ESI-MS: cacld for $[M + H]^+$ m/z = 775.3482, found m/z = 775.3486.

Synthesis of (1-(*N*-Boc-3-aminopropyl)-1*H*-1,2,3-triazol-4-yl) methyleneoxy-P5A (HT-Boc). 0.57 g (0.74 mmol) propargyl-P5A were suspended in 100 ml MeCN in a 250 ml three-necked flask at 50 °C. 0.2 ml (1.5 mmol, 2 eq.) Et_3N were added to the mixture followed by addition of 95 mg (0.5 mmol; 0.67 eq.) CuI solution in 6 ml MeCN. After stirring for 15 min the mixture turned yellow and 154 mg (0.77 mmol, 1.04 eq.) BAPA were added resulting in disappearance of the color of the solution. The reaction was controlled by TLC (SiO_2 plates, 100% DCM). After 20 h the reaction was complete, the solvent removed *in vacuo*, the residue was resolved in 80 ml DCM and washed

with 80 ml diluted (0.05 M) HCl. An insoluble brown precipitation formed during washing was filtered out, the organic phase of the filtrate was isolated, and DCM was removed *in vacuo*. The crude product was purified by column chromatography (SiO_2; DCM : MeOH 100 : 0 to 100 : 1). HT-Boc was obtained as colorless film (0.5448 g; 0.56 mmol; 76%).

T_{mp} = 159–171 °C.

^{1}H NMR‡ (700 MHz, MeCN-d_3 : $CDCl_3$ 3 : 1) δ (ppm) = 7.89 (br s, 1H, triazole C**H**); 7.02, 6.92, 6.91, 6.90, 6.89, 6.89, 6.88, 6.87, 6.86, 6.80 (s, 10H, C_{Ar}–**H**); 5.33 (br s, 1H, N**H**); 5.03 (s, 2H, O–C$\mathbf{H}_2$–C(–N)=CH); 4.38 (br tr, $^3J_{HH}$ = 6.2 Hz; 2H, N=N–N–C$\mathbf{H}_2$); 3.76–3.66, 3.56 (m, 37H, O–C$\mathbf{H}_3$ and C_{Ar}–C$\mathbf{H}_2$); 3.07 (m, 2H, NH–C$\mathbf{H}_2$); 2.03 (m, 2H, NH–CH_2–C$\mathbf{H}_2$); 1.41 (s, 9H, C–C$\mathbf{H}_3$).

^{13}C NMR‡ (176 MHz, MeCN-d_3 : $CDCl_3$ 3 : 1) δ (ppm) = 156.9 (**C**=O); 151.5, 151.0, 151.0, 150.9, 149.7 ($\mathbf{C}_{Ar}$–O); 145.0 ($\mathbf{C}_{triaz}$–CH_2); 130.0, 129.3, 129.3, 129.2 ($\mathbf{C}_{Ar}$–CH_2); 124.3 ($\mathbf{C}_{triaz}$–H); 115.5, 114.1, 114.0, 113.9, 113.9, 113.9, 113.9, 113.8, 113.8 ($\mathbf{C}_{Ar}$–H); 79.3 ($\mathbf{C}(CH_3)_3$); 63.4 (O–$\mathbf{C}H_2$); 56.3, 56.3, 56.3, 56.2, 56.1, 56.1 (O–$\mathbf{C}H_3$); 48.4 (triazol–$\mathbf{C}H_2$); 38.1 (NH–$\mathbf{C}H_2$); 31.4 (NH–CH_2–$\mathbf{C}H_2$); 29.8, 29.8, 29.7 (C_{Ar}–$\mathbf{C}H_2$); 28.7 (C($\mathbf{C}H_3)_3$).

ESI-MS: cacld for $[M + H]^+$ m/z = 975.4750, found m/z = 975.4777. Cacld for $[M + Na]^+$ m/z = 997.4575, found m/z = 997.4599.

Synthesis of (1-(3-aminopropyl)-1*H*-1,2,3-triazol-4-yl) methyleneoxy-P5A hydrochloride (HT). 0.5 g (0.51 mmol) HT-Boc were dissolved in 4 ml 1,4-dioxane followed by addition of 2 ml 4 M HCl in 1,4-dioxane. The mixture was stirred overnight, then evaporated *in vacuo* to give HT in a quantitative yield as a yellow film-like solid in a quantitative yield.

^{1}H NMR§ (700 MHz, MeCN-d_3 : $CDCl_3$ 3 : 1) δ (ppm) = 8.04 (s, 1H, C_{triaz}–**H**); 7.90 (br s, 3H, N$\mathbf{H}_3^+$); 7.03, 6.91, 6.90, 6.89, 6.89, 6.88, 6.88, 6.87, 6.86, 6.81 (s, 10H, C_{Ar}–**H**); 5.03 (s, 2H, O–C$\mathbf{H}_2$); 4.57 (tr, $^3J_{HH}$ = 6.4 Hz; 2H, triazol–C$\mathbf{H}_2$); 3.77–3.65, 3.57 (m, 37H, O–C$\mathbf{H}_3$ and C_{Ar}–C$\mathbf{H}_2$); 3.03 (m, 2H, NH_3^+–C$\mathbf{H}_2$); 2.39 (quint, $^3J_{HH}$ = 6.1 Hz; 2H, NH_3^+–CH_2–C$\mathbf{H}_2$).

^{13}C NMR§ (176 MHz, MeCN-d_3 : $CDCl_3$ 3 : 1) δ (ppm) = 151.5, 151.0, 151.0, 150.9, 149.6 ($\mathbf{C}_{Ar}$–O); 145.5 ($\mathbf{C}_{triaz}$–CH_2); 130.0, 129.3, 129.3, 129.3, 129.3, 129.2, 129.1 ($\mathbf{C}_{Ar}$–CH_2); 125.0 ($\mathbf{C}_{triaz}$–H); 115.5, 114.1, 113.9, 113.9, 113.9, 113.9, 113.8, 113.7 ($\mathbf{C}_{Ar}$–H); 63.2 (O–$\mathbf{C}H_2$); 56.4, 56.3, 56.3, 56.3, 56.2, 56.1, 56.0 ($\mathbf{C}H_3$); 48.0 (triazol–$\mathbf{C}H_2$); 38.1 (NH_3^+–$\mathbf{C}H_2$); 29.9, 29.8, 29.7, 29.7 (C_{Ar}–$\mathbf{C}H_2$); 28.5 (NH_3^+–CH_2–$\mathbf{C}H_2$).

ESI-MS: cacld for $[M + H]^+$ m/z = 875.4226, found m/z = 875.4221.

Synthesis of 3-(6-((*tert*-butyloxycarbonyl)amino)hexyl)-1-methyl-1*H*-imidazol-3-ium bromide (MIHA-Boc). To the 0.3 g (3.66 mmol) 1-methyl-1*H*-imidazole in a dry Schlenk tube 985.4 mg (3.517 mmol) BBHA were slowly added at cooling on the ice bath. The mixture was stirred for 1 h at 0 °C, then 144 h at RT. Further, the reaction mixture was diluted with ethanol and a small excess of BBHA was added to ensure a full conversion of the 1-methyl-1*H*-imidazole. The solution was therefore stirred additional 16 h at 50 °C followed by solvent evaporation *in vacuo*. The crude product was dissolved in 30 ml water and washed with EtOAc (30 ml). The aqueous phase was collected, the solvent was removed by rotary evaporator, and the product was dried *in vacuo*. MIHA-Boc (1.03 g; 2.83 mmol; 81%) was obtained as a viscous yellowish liquid.

^{1}H NMR (700 MHz, $CDCl_3$) δ (ppm) = 10.45 (s, 1H, N=C**H**–N), 7.40 (m, 1H, CH_3–N–C**H**=CH), 7.38 (m, 1H, CH_3–N–CH=C**H**), 4.71 (s, 1H, N**H**), 4.33 (t, $^3J_{HH}$ = 7.3 Hz, 2H, imidazolyl–C$\mathbf{H}_2$), 4.11 (s, 3H, N$^-$C$\mathbf{H}_3$), 3.07 (t, $^3J_{HH}$ = 6.3 Hz, 2H, NH–C$\mathbf{H}_2$), 1.92 (m, 2H, imidazolyl–CH_2–C$\mathbf{H}_2$), 1.47 (m, 2H, NH–CH_2–C$\mathbf{H}_2$), 1.41 (s, 9H, C(C$\mathbf{H}_3)_3$), 1.36 (m, 4H, imidazolyl–CH_2–CH_2–C$\mathbf{H}_2$ and NH–CH_2–CH_2–C$\mathbf{H}_2$).

^{13}C NMR (176 MHz, $CDCl_3$) δ (ppm) = 156.3 (**C**=O), 138.1 (N=**C**H–N), 123.4 (CH_3–N–**C**H=CH), 122.0 (CH_3–N–CH=**C**H), 79.3 (**C**($CH_3)_3$), 50.2 (imidazolyl–**C**H_2), 40.3 (NH–**C**H_2), 37.0 (N–**C**H_3), 30.2 (imidazolyl–CH_2–**C**H_2), 29.9 (NH–CH_2–**C**H_2), 28.6 (C(**C**$H_3)_3$), 26.0 (imidazolyl–CH_2–CH_2–**C**H_2), 25.8 (NH–CH_2–CH_2–**C**H_2).

ESI-MS: cacld for $[M]^+$ m/z = 282.2176, found m/z = 282.2178.

Synthesis of 1-(6-ammoniohexyl)-3-methyl-1*H*-imidazol-3-ium (chloride/bromide) (MIHA). To the solution of 0.52 g (1.42 mmol) MIHA-Boc in 5 ml 1,4-dioxane 3.5 ml HCl (4M in 1,4-dioxane; 14.21 mmol) were added and the mixture was stirred for 3 h at RT. The solvent was evaporated, and the product was dried *in vacuo*. MIHA (0.38 g; 1.27 mmol; 89%) was obtained as a hygroscopic solid.

^{1}H NMR (700 MHz, D_2O) δ (ppm) = 8.69 (m, 1H, N=C**H**–N); 7.46 (m, 1H, CH_3–N–C**H**=CH); 7.41 (m, 1H, CH_3–N–CH=C**H**); 4.18 (t, $^3J_{HH}$ = 7.2 Hz, 2H, imidazolyl–C$\mathbf{H}_2$); 3.87 (s, 3H, N–C$\mathbf{H}_3$); 2.97 (t, $^3J_{HH}$ = 7.6 Hz, 2H, NH_3^+–C$\mathbf{H}_2$); 1.87 (tt, $^3J_{HH}$ = 7.5 Hz, 2H, imidazolyl–CH_2–C$\mathbf{H}_2$); 1.64 (tt, $^3J_{HH}$ = 7.7 Hz, 2H, NH_3^+–CH_2–C$\mathbf{H}_2$); 1.40 (tt, $^3J_{HH}$ = 7.4 Hz, 2H, NH_3^+–CH_2–CH_2–C$\mathbf{H}_2$); 1.33 (tt, $^3J_{HH}$ = 7.4 Hz, 2H, triazolyl–CH_2–CH_2–C$\mathbf{H}_2$).

^{13}C NMR (176 MHz, D_2O) δ (ppm) = 135.8 (N=**C**H–N); 123.5 (CH_3–N–CH=**C**H); 122.1 (CH_3–N–**C**H=CH); 49.3 (imidazolyl–**C**H_2); 39.3 (NH_3^+–**C**H_2); 35.6 (N–**C**H_3); 29.0 (imidazolyl–CH_2–**C**H_2); 26.5 (NH_3^+–CH_2–**C**H_2); 25.0 (NH_3^+–CH_2–CH_2–**C**H_2); 24.9 (imidazolyl–CH_2–CH_2–**C**H_2).

ESI-MS: cacld for $[M]^+$ m/z = 182.1652, found m/z = 182.1631.

Synthesis of 1-(6-((*tert*-butyloxycarbonyl)amino)hexyl)-pyridin-1-ium bromide (PHA-Boc). To 0.753 g (2.69 mmol) BBHA in a round-bottom flask 0.4 ml (0.393 g; 4.97 mmol) pyridine were added followed by stirring for 24 h at 80 °C. Subsequently, the mixture was diluted in 15 ml EtOH and evaporated. The product was dried *in vacuo*. PHA-Boc (0.765 g; 2.13 mmol; 79%) was obtained as an orange film.

^{1}H NMR (700 MHz, $CDCl_3$) δ (ppm) = 9.55 (m, 2H, C$\mathbf{H}_{ortho}$); 8.52 (dd, $^3J_{HH}$ = 7.8 Hz, 1H, C$\mathbf{H}_{para}$); 8.13 (dd, $^3J_{HH}$ = 6.9 Hz; 2H, C$\mathbf{H}_{metha}$); 4.99 (t, $^3J_{HH}$ = 7.2 Hz, 2H, Py–C$\mathbf{H}_2$); 4.79 (s, 1H,

‡ The compound HT-Boc is inclined to formation of inter- or even intramolecular inclusion complexes in $CDCl_3$, where the side chain acts as a guest moiety for the macrocycle. For this reason, CD_3CN was used as a co-solvent for the analysis.
§ The compound HT is inclined to formation of inter- or even intramolecular inclusion complexes in $CDCl_3$, where the side chain acts as a guest moiety for the macrocycle. For this reason, CD_3CN was used as a co-solvent for the analysis.

NH); 3.03 (m, 2H, NH–CH$_2$); 2.05 (m, 2H, Py–CH$_2$–CH$_2$); 1.44 (m, 2H, NH–CH$_2$–CH$_2$); 1.39 (s, 9H, C(CH$_3$)$_3$); 1.35 (m, 4H, Py–CH$_2$–CH$_2$–CH$_2$ und NH–CH$_2$–CH$_2$–CH$_2$).

^{13}C NMR (176 MHz, CDCl$_3$) δ (ppm) = 156.3 (C=O); 145.4 (CH$_{para}$); 145.4 (CH$_{ortho}$); 128.6 (CH$_{meta}$); 79.2 (C(CH$_3$)$_3$); 61.9 (Py–CH$_2$); 40.3 (NH–CH$_2$); 32.0 (Py–CH$_2$–CH$_2$); 29.8 (NH–CH$_2$–CH$_2$); 28.6 (C(CH$_3$)$_3$); 26.1 (NH–CH$_2$–CH$_2$–CH$_2$); 25.6 (Py–CH$_2$–CH$_2$–CH$_2$).

ESI-MS: cacld for [M]$^+$ m/z = 279.2067, found m/z = 279.2082.

Synthesis of 1-(6-((*tert*-butyloxycarbonyl)amino)hexyl)-1*H*-1,2,4-triazole (THA-Boc). 2.52 g BBHA (9.0 mmol) was placed in a 250 ml round-bottom flask followed by the addition of 623 mg (9.0 mmol) 1*H*-1,2,4-triazole in 15 ml THF. The flask was sealed with a septum and cooled down to 0 °C on the ice bath. 1.933 g (12.6 mmol) DBU in 4 ml THF were added dropwise over 15 min. The mixture was stirred for an hour at cooling, then 16 h at RT. The formed precipitate was filtered out and washed with THF (10 ml) on the frit. The filtrate was evaporated to obtain an orange oil as a crude product. The oil was dissolved in 50 ml EtOAc and washed with 50 ml H_2O, the aqueous phase was extracted with 30 ml EtOAc and the combined organic phases were dried over $MgSO_4$. The product was isolated by column chromatography on silica gel (EtOAc 100%). The evaporation of the solvent gave THA-Boc as a transparent viscous liquid which crystallized into white solid after several months (1.52 g; 5.7 mmol; 63%).

T_{mp} = 61 °C.

^{1}H NMR (700 MHz, CDCl$_3$) δ (ppm) = 8.06 (s, 1H, H5$_{triazole}$), 7.93 (s, 1H, H3$_{triazole}$), 4.53 (br s, 1H, NH), 4.15 (t, $^3J_{HH}$ = 7.1 Hz; 2H, triazolyl–CH$_2$), 3.09 (m, 2H, NH–CH$_2$), 1.88 (quint, $^3J_{HH}$ = 7.3 Hz; 2H, triazolyl–CH$_2$–CH$_2$), 1.45 (m, 2H, NH–CH$_2$–CH$_2$), 1.43 (s, 9H, CH$_3$), 1.37–1.27 (m, 4H, NH–CH$_2$–CH$_2$–CH$_2$–CH$_2$).

^{13}C NMR (176 MHz, CDCl$_3$) δ (ppm) = 156.2 (C=O), 152.0 (C3$_{triazole}$), 143.0 (C5$_{triazole}$), 79.3 (C(CH$_3$)$_3$), 49.8 (triazolyl–CH$_2$), 40.5 (NH–CH$_2$), 30.1 (NH–CH$_2$–CH$_2$), 29.9 (triazolyl–CH$_2$–CH$_2$), 28.6 (CH$_3$), 26.3, 26.3 (NH–CH$_2$–CH$_2$–CH$_2$–CH$_2$).

ESI-MS: cacld for [M + Na]$^+$ m/z = 291.1797, found m/z = 291.1784.

Synthesis of 1-(6-((*tert*-butyloxycarbonyl)amino)hexyl)-1*H*-imidazole (IHA-Boc). Solution of 1.02 g (3.64 mmol) BBHA in 6 ml THF was combined with a solution of 0.25 g (3.63 mmol) imidazole in 5 ml THF in a round-bottom flask. To the mixture a solution of 0.84 g (5.53 mmol) DBU in 3 ml THF was added dropwise over 15 min at 0 °C. The reaction mixture was stirred for 1 h at cooling and 144 h at 55 °C. A precipitate formed upon addition of 30 ml EtOAc was removed by filtration, and the solvent from the filtrate was removed *in vacuo*. The residue was resolved in EtOAc (40 ml) and washed with water (50 ml). The aqueous phase was extracted once again with 40 ml EtOAc, and the combined organic phases were dried over Na_2SO_4. The solvent was removed by evaporation, and the product was purified by column chromatography (SiO_2; 100% EtOAc) followed by drying *in vacuo*. IHA-Boc (0.14 g; 0.52 mmol; 14%) was obtained as a colorless film.

^{1}H NMR (700 MHz, CDCl$_3$) δ (ppm) = 7.49 (s, 1H, N=CH–N); 7.06 (s, 1H, CH$_2$–N–CH=CH); 6.90 (s, 1H, CH$_2$–N–CH=CH); 4.51 (s, 1H, NH); 3.92 (t, $^3J_{HH}$ = 7.1 Hz, 2H, imidazolyl–CH$_2$); 3.09 (m, 2H, NH–CH$_2$); 1.78 (tt, $^3J_{HH}$ = 7.2 Hz, 2H, imidazolyl–CH$_2$–CH$_2$); 1.46 (m, 2H, NH–CH$_2$–CH$_2$); 1.43 (m, 9H, C(CH$_3$)$_3$); 1.32 (m, 4H, imidazolyl–CH$_2$–CH$_2$–CH$_2$ and NH–CH$_2$–CH$_2$–CH$_2$).

^{13}C NMR (176 MHz, CDCl$_3$) δ (ppm) = 156.2 (C=O); 137.2 (N=CH–N); 129.4 (CH$_2$–N–CH=CH); 119.0 (CH$_2$–N–CH=CH); 79.4 (C(CH$_3$)$_3$); 47.2 (imidazolyl–CH$_2$); 40.6 (NH–CH$_2$); 31.2 (imidazolyl–CH$_2$–CH$_2$); 30.2 (NH–CH$_2$–CH$_2$); 28.6 (C(CH$_3$)$_3$); 26.4 (imidazolyl–CH$_2$–CH$_2$–CH$_2$ and NH–CH$_2$–CH$_2$–CH$_2$).

ESI-MS: cacld for [M + H]$^+$ m/z = 268.2020, found m/z = 268.2011.

Synthesis of 6-((*tert*-butoxycarbonyl)amino)-*N*,*N*,*N*-trimethylhexan-1-aminium bromide (TAHA-Boc). In a 25 ml flask 1.0 g (3.57 mmol) BBHA was dissolved in 10 ml EtOH, 1.6 ml NMe$_3$ solution in EtOH (4.2 M, 33%; 6.7 mmol) were added to the solution. The flask was sealed and placed onto an oil bath at 50 °C for 20 h. Then, the solvent and the unreacted NMe$_3$ were evaporated *in vacuo*, followed by careful drying *in vacuo* at 80 °C to remove EtOH completely. TAHA-Boc was obtained as white crystalline solid and was reacted further *in situ*.

^{1}H NMR (700 MHz, DMSO-d$_6$) δ (ppm) = 6.78 (t, $^3J_{HH}$ = 5.5 Hz, 1H, NH), 3.27 (m, 2H, Me$_3$N$^+$–CH$_2$), 3.05 (s, 9H, N$^+$(CH$_3$)$_3$), 2.90 (dt, 2H, NH–CH$_2$), 1.65 (m, 2H, Me$_3$N$^+$–CH$_2$–CH$_2$), 1.43–1.32 (m, 11H, NH–CH$_2$–CH$_2$ and C(CH$_3$)$_3$), 1.32–1.21 (m, 4H, Me$_3$N$^+$–CH$_2$–CH$_2$–CH$_2$ and NH–CH$_2$–CH$_2$–CH$_2$).

^{13}C NMR (176 MHz, DMSO-d$_6$) δ (ppm) = 155.5 (C=O), 77.3 (C(CH$_3$)$_3$), 65.2 (Me$_3$N$^+$–CH$_2$), 52.1 (N$^+$(CH$_3$)$_3$), 39.6 (NH–CH$_2$), 29.2 (NH–CH$_2$–CH$_2$), 28.3 (CH$_3$), 25.7, 25.4 (Me$_3$N$^+$–CH$_2$–CH$_2$–CH$_2$ and NH–CH$_2$–CH$_2$–CH$_2$), 22.0 (Me$_3$N$^+$–CH$_2$–CH$_2$).

ESI-MS: cacld for [M]$^+$ m/z = 259.2386, found m/z = 259.2363.

Synthesis of poly(DMAAm-*co*-VDMA). In a pre-heated Schlenk-tube 0.0115 g (0.032 mmol) 2-(dodecylthiocarbonothioylthio)-2-methylpropionic acid, 2.00 g (20.18 mmol) dimethyl acrylamide and 0.698 g (5.02 mmol) VDMA were dissolved in 5 ml 1,4-dioxane and to the solution 0.0026 g (0.016 mmol) AIBN in 1 ml 1,4-dioxane were added. The Schlenk-tube was sealed with a septum, and the mixture was degassed by purging with Ar for 30 min before being placed onto an oil bath at 70 °C. After 16 h the reaction was quenched by freezing the mixture in liquid nitrogen and exposing it to the air. After the solution has thawed, it was diluted with 6 ml THF and precipitated into 150 ml Et_2O (cooled by acetone/N_2 bath). The supernatant was decanted, and the precipitate was resolved in 10 ml THF followed by precipitation in 300 ml Et_2O at RT. The precipitated was isolated by filtration and dried *in vacuo*. Poly(DMAAm-*co*-VDMA) was obtained as a white solid (2.262 g; 83%).

^{1}H NMR (500 MHz, CDCl$_3$) δ (ppm) = 3.62–2.71 (m, 2850H, N(CH$_3$)$_2$); 2.71–2.14 (m, 540H, backbone–CH); 2.14–0.90 (m, 1720H, backbone–CH$_2$ and VDMA–CH$_3$); 0.87 (t, $^3J_{HH}$ = 7.0 Hz; 3H, S-C$_{11}$H$_{22}$-CH$_3$).

SEC: M_n = 53 400, $Đ$ = 1.90.

Synthesis of HT- and DMIEA-modified p(DMAAm-*co*-VDMA) (PHTP). To 0.100 g poly(DMAAm-*co*-VDMA) in a pear-shaped flask two solutions were added: a solution of HT (0.132 g; 0.145 mmol) with DBU (0.091 g; 0.598 mmol) in 5 ml DMF and a solution of DMIEA (0.010 g; 0.049 mmol) with DBU (0.030 g; 0.197 mmol) in 2 ml DMF. The reaction mixture was stirred in dark under Ar at RT for 20 h followed by addition of 0.12 ml (1.90 mmol) ethanolamine and subsequent stirring for 1 h. The mixture was precipitated into 100 ml Et_2O at RT and the precipitate isolated by filtration. The crude product was resolved in 20 ml acetone, the solution dialyzed in water for 24 h and freeze-dried to obtain PHTP (0.180 g; 76%) as a white solid.

^{1}H NMR (500 MHz, $CDCl_3$) δ (ppm) = 8.00–7.56 (br, 1H, triazole C**H**); 6.89, 6.82–6.62 (br s, 10H, P5A C$\mathbf{H}_{Ar}$), 5.00 (s, 2H, O–C$\mathbf{H}_2$–C(–N)=CH); 4.41 (br, 2H, N=N–N–C$\mathbf{H}_2$); 3.82–3.70 (br s, 10H, P5A C_{Ar}–C$\mathbf{H}_2$); 3.70–3.53, 3.48 (br s, 27H, P5A O–C$\mathbf{H}_3$); 3.23–2.74 (m, 52H, N(C$\mathbf{H}_3$)$_2$); 2.74–2.27 (m, 10H, backbone C**H**); 2.27–0.92 (m, 48H, backbone C$\mathbf{H}_2$, C(=O)–NH–C(C$\mathbf{H}_3$)$_2$, C(C$\mathbf{H}_3$)=C(C$\mathbf{H}_3$), C(=O)–NH–C$\mathbf{H}_2$–C$\mathbf{H}_2$).

SEC: M_n = 103 200, $Đ$ = 2.21.

Synthesis of MIHA- and DMIEA-modified p(DMAAm-*co*-VDMA) (PMIHAP). To 0.200 g poly(DMAAm-*co*-VDMA) in a pear-shaped flask two solutions were added: a solution of MIHA (0.078 g; 0.306 mmol) with DBU (0.084 g; 0.552 mmol) in 5 ml DMF and a solution of DMIEA (0.020 g; 0.098 mmol) with DBU (0.041 g; 0.269 mmol) in 1.5 ml DMF. The reaction mixture was stirred at RT for 20 h followed by addition of 0.12 ml (1.90 mmol) ethanolamine and subsequent stirring for 1 h. The mixture was precipitated into 100 ml Et_2O at RT and the precipitate isolated by filtration. The crude product was resolved in 10 ml water, and the solution dialyzed in water for 24 h. The solvent was evaporated *in vacuo* to obtain PMIHAP (0.243 g; 87%) as a white solid.

^{1}H NMR (500 MHz, D_2O) δ (ppm) = 7.51 (s, 1H, CH_3–N–CH=C**H**–N); 7.47 (s, 1H, CH_3–N–C**H**=CH–N); 4.22 (t, $^3J_{HH}$ = 6.8 Hz; 2H, CH_3–$C_3H_3N_2^+$–C$\mathbf{H}_2$); 3.92 (s, 3H, C$\mathbf{H}_3$–$C_3H_3N_2^+$); 3.30–2.84 (m, 48H, N(C$\mathbf{H}_3$)$_2$ and $C_3H_3N_2^+$–C_5H_{10}–C$\mathbf{H}_2$); 2.84–2.35 (m, 8H, backbone C**H**); 1.96 (s, 1H, C(C$\mathbf{H}_2$)=C(C$\mathbf{H}_2$)); 1.88 (br, 2H, $C_3H_3N_2^+$–CH_2–C$\mathbf{H}_2$); 1.85–1.14 (m, 35H, backbone C$\mathbf{H}_2$, C(=O)–NH–C(C$\mathbf{H}_3$)$_2$ and $C_3H_3N_2^+$–CH_2–CH_2–C$\mathbf{H}_2$–C$\mathbf{H}_2$–C$\mathbf{H}_2$).

SEC: M_n = 68 900, $Đ$ = 2.57.

Conclusions

In this work, we constructed a sensor chip for the detection of adiponitrile based on a dually crosslinked gel. Chemical crosslinks formed by dimerization of DMIEA endowed the network with stability, whereas supramolecular host–guest complexes with P5A acted as reversible crosslinks disrupted upon presence of AN, due to the competitive complexation between the moieties. For the design of the gel MIHA was selected as a guest moiety from various neutral and positively charged amine- and heterocycle-substituted aminohexanes. The selection was conducted by the evaluation of the binding affinity of Boc-protected axles with P5A. NMR titration revealed that K_a of MIHA-Boc and PHA-Boc with the macrocycle are by one order of magnitude higher than those of THA-Boc and TAHA-Boc complexes, while still being lower than K_a of the AN@P5A complex. IHA-Boc was found to form complex of 1 : 2 (H : G) stoichiometry with P5A. Additionally, it was demonstrated using 2D DOSY NMR that for neither fast nor slow exchange complexes the mobility of the bound species is fully reduced to the mobility of P5A. The diffusion coefficient, therefore, stays an average between free and "completely bound" states. HT as a host moiety was synthesized by a mono-demethylation of P5A and further etherification of the phenolic OH-group.

Host and guest polymers were synthesized by modification of a P0 copolymer containing VDMA as a comonomer with HT, MIHA (which was our guest moiety of choice) and a photocrosslinker. By spin-coating and subsequent curing under UV-irradiation, a thin gel layer was fabricated, which was treated with $CHCl_3$ and AN solution of different concentrations (1 μM up to 1 mM). By measuring the change in swelling degree and refractive index using SPR technique, a limit of detection was estimated as a sensitivity parameter of the sensor chip (LoD = 25 μM). Thus, the designed polymeric gel system can serve as a starting point for the development of a sensor for adiponitrile as well as other small molecules capable of forming stable complexes with pillar[*n*]arenes. We believe that further tuning of the polymer parameters as well as methodology will help improve the performance of the sensing platform for the fabrication of sensors in a form of devices.

Author contributions

Maksim Rodin: conceptualization, investigation, formal analysis, writing – original draft. David Helle: investigation, formal analysis. Dirk Kuckling: conceptualization, writing – review & editing, supervision, project administration.

Conflicts of interest

There are no conflicts to declare.

Acknowledgements

The authors gratefully acknowledge financial support from the Deutsche Forschungsgemeinschaft (DFG, 501220359).

References

1 L. Voorhaar and R. Hoogenboom, *Chem. Soc. Rev.*, 2016, **45**, 4013–4031.
2 C. Creton, *Macromolecules*, 2017, **50**, 8297–8316.
3 X. Huang, R. Li, Z. Duan, F. Xu and H. Li, *Soft Matter*, 2022, **18**, 3828–3844.

4 A. D. O'Donnell, S. Salimi, L. R. Hart, T. S. Babra, B. W. Greenland and W. Hayes, *React. Funct. Polym.*, 2022, **172**, 105209.
5 S. L. Craig, *Angew. Chem., Int. Ed.*, 2009, **48**, 2645–2647.
6 M. A. Aboudzadeh, M. E. Muñoz, A. Santamaría, R. Marcilla and D. Mecerreyes, *Macromol. Rapid Commun.*, 2012, **33**, 314–318.
7 Y. Sun, Y.-Y. Ren, Q. Li, R.-W. Shi, Y. Hu, J.-N. Guo, Z. Sun and F. Yan, *Chin. J. Polym. Sci.*, 2019, **37**, 1053–1059.
8 J. Sautaux, F. Marx, I. Gunkel, C. Weder and S. Schrettl, *Nat. Commun.*, 2022, **13**, 356.
9 M. Ahmadi, A. Jangizehi and S. Seiffert, *Macromolecules*, 2022, **55**, 5514–5526.
10 Z. Jing, X. Huang, X. Liu, M. Liao and Y. Li, *Polym. Int.*, 2023, **72**, 39–53.
11 X. Yang, R. Bai, Z. Zhang, Y. Liu and X. Yan, *J. Polym. Sci.*, 2023, **61**, 1105–1110.
12 J. Park, Y. Sasaki, Y. Ishii, S. Murayama, K. Ohshiro, K. Nishiura, R. Ikura, H. Yamaguchi, A. Harada, G. Matsuba, H. Washizu, T. Minami and Y. Takashima, *ACS Appl. Mater. Interfaces*, 2023, **15**, 39777–39785.
13 K. Belal, F. Stoffelbach, D. Hourdet, A. Marcellan, J. Lyskawa, L. de Smet, A. Vebr, J. Potier, G. Cooke, R. Hoogenboom and P. Woisel, *Macromolecules*, 2021, **54**, 1926–1933.
14 Y. Guo, Y. Liu, X. Zhao, J. Zhao, Y. Wang, X. Zhang, Z. Guo and X. Yan, *ACS Appl. Mater. Interfaces*, 2023, **15**, 25161–25172.
15 Y. Zhao, Z. Li, Q. Li, L. Yang, H. Liu, R. Yan, L. Xiao, H. Liu, J. Wang, B. Yang and Q. Lin, *Macromol. Rapid Commun.*, 2020, **41**, e2000441.
16 P. Chakraborty, H. Oved, D. Bychenko, Y. Yao, Y. Tang, S. Zilberzwige-Tal, G. Wei, T. Dvir and E. Gazit, *Adv. Mater.*, 2021, **33**, e2008715.
17 Y. Liang, Z. Li, Y. Huang, R. Yu and B. Guo, *ACS Nano*, 2021, **15**, 7078–7093.
18 Y. Zhao, S. Song, X. Ren, J. Zhang, Q. Lin and Y. Zhao, *Chem. Rev.*, 2022, **122**, 5604–5640.
19 S. J. K. O'Neill, Z. Huang, M. H. Ahmed, A. J. Boys, S. Velasco-Bosom, J. Li, R. M. Owens, J. A. McCune, G. G. Malliaras and O. A. Scherman, *Adv. Mater.*, 2023, **35**, e2207634.
20 G. Su, S. Yin, Y. Guo, F. Zhao, Q. Guo, X. Zhang, T. Zhou and G. Yu, *Mater. Horiz.*, 2021, **8**, 1795–1804.
21 C. B. Rodell, R. J. Wade, B. P. Purcell, N. N. Dusaj and J. A. Burdick, *ACS Biomater. Sci. Eng.*, 2015, **1**, 277–286.
22 M. Tao, K. Xu, S. He, H. Li, L. Zhang, X. Luo and W. Zhong, *Chem. Commun.*, 2018, **54**, 4673–4676.
23 S. Bernhard and M. W. Tibbitt, *Adv. Drug Delivery Rev.*, 2021, **171**, 240–256.
24 G. Zhang, J. Li, W. Cai, S. Li, Y. Kong and Z.-Z. Yin, *Microchem. J.*, 2023, **193**, 109160.
25 M. I. Rial-Hermida, D. C. S. Costa, L. Jiang, J. M. M. Rodrigues, K. Ito and J. F. Mano, *Gels*, 2023, **9**(2), 85.
26 R. Ikura, J. Park, M. Osaki, H. Yamaguchi, A. Harada and Y. Takashima, *NPG Asia Mater.*, 2022, **14**, 10.
27 K. Belal, F. Stoffelbach, J. Lyskawa, M. Fumagalli, D. Hourdet, A. Marcellan, L. de Smet, V. R. de La Rosa, G. Cooke, R. Hoogenboom and P. Woisel, *Angew. Chem., Int. Ed.*, 2016, **55**, 13974–13978.
28 M. Mauro, *J. Mater. Chem. B*, 2019, **7**, 4234–4242.
29 D. Tian, W. Ma, L. Zheng, K. Jiang, H. He and R. Sun, *ACS Appl. Polym. Mater.*, 2023, **5**, 8641–8649.
30 Z. Huang, X. Chen, S. J. K. O'Neill, G. Wu, D. J. Whitaker, J. Li, J. A. McCune and O. A. Scherman, *Nat. Mater.*, 2022, **21**, 103–109.
31 X. Ji, Y. Yao, J. Li, X. Yan and F. Huang, *J. Am. Chem. Soc.*, 2013, **135**, 74–77.
32 M. Rodin, J. Li and D. Kuckling, *Chem. Soc. Rev.*, 2021, **50**, 8147–8177.
33 L. Hammer, N. J. van Zee and R. Nicolaÿ, *Polymers*, 2021, **13**(3), 396.
34 J. Chen, Q. Su, R. Guo, J. Zhang, A. Dong, C. Lin and J. Zhang, *Macromol. Chem. Phys.*, 2017, **218**, 1700166.
35 G. Davidson-Rozenfeld, L. Stricker, J. Simke, M. Fadeev, M. Vázquez-González, B. J. Ravoo and I. Willner, *Polym. Chem.*, 2019, **10**, 4106–4115.
36 C. Qian, T.-A. Asoh and H. Uyama, *Macromol. Rapid Commun.*, 2020, **41**, e2000406.
37 Y. Liu, L. Wang, H. Lu and Z. Huang, *Chem. Eng. J.*, 2022, **431**, 133338.
38 J. Deng, R. Bai, J. Zhao, G. Liu, Z. Zhang, W. You, W. Yu and X. Yan, *Angew. Chem., Int. Ed.*, 2023, **62**, e202309058.
39 N. Liubimtsev, Z. Zagradska-Paromova, D. Appelhans, J. Gaitzsch and B. Voit, *Macromol. Chem. Phys.*, 2023, **224**(3), 2200372.
40 J. Li, C. Ji, X. Yu, M. Yin and D. Kuckling, *Macromol. Rapid Commun.*, 2019, **40**, e1900189.
41 J. Li, C. Ji, B. Lü, M. Rodin, J. Paradies, M. Yin and D. Kuckling, *ACS Appl. Mater. Interfaces*, 2020, **12**, 36873–36881.
42 A. Azzouz, L. Hejji, K.-H. Kim, D. Kukkar, B. Souhail, N. Bhardwaj, R. J. C. Brown and W. Zhang, *Biosens. Bioelectron.*, 2022, **197**, 113767.
43 J. Kümper, J. Meyers, R. Sebers, N. Kurig and R. Palkovits, *Green Chem.*, 2023, **25**, 6231–6237.
44 D. E. Blanco, A. Z. Dookhith and M. A. Modestino, *React. Chem. Eng.*, 2019, **4**, 8–16.
45 V. Vaks, V. Anfertev, M. Chernyaeva, E. Domracheva, A. Yablokov, A. Maslennikova, A. Zhelesnyak, A. Baranov, Y. Schevchenko and M. F. Pereira, *Sci. Rep.*, 2022, **12**, 18117.
46 R. A. Woutersen, *Scand. J. Work, Environ. Health*, 1998, **24**, 5–9.
47 D. Coggon and P. Cole, *Scand. J. Work, Environ. Health*, 1998, **24**, 81–82.
48 S. Caito, Y. Yu and M. Aschner, *NeuroToxicology*, 2013, **37**, 93–99.
49 R. D. Short, W. V. Roloff, L. D. Kier and W. E. Ribelin, *J. Toxicol. Environ. Health*, 1990, **30**, 199–207.

50 G. L. Kennedy, *Drug Chem. Toxicol.*, 2004, **27**, 123–131.
51 B. Shi, L. Shangguan, H. Wang, H. Zhu, H. Xing, P. Liu, Y. Liu, J. Liu and F. Huang, *ACS Mater. Lett.*, 2019, **1**, 111–115.
52 T. Ogoshi, S. Kanai, S. Fujinami, T. Yamagishi and Y. Nakamoto, *J. Am. Chem. Soc.*, 2008, **130**, 5022–5023.
53 T. Ogoshi, T. Yamagishi and Y. Nakamoto, *Chem. Rev.*, 2016, **116**, 7937–8002.
54 X. Shu, J. Fan, J. Li, X. Wang, W. Chen, X. Jia and C. Li, *Org. Biomol. Chem.*, 2012, **10**, 3393–3397.
55 Y. Wang, G. Ping and C. Li, *Chem. Commun.*, 2016, **52**, 9858–9872.
56 X. Lou, H. Chen, X. Jia and C. Li, *Chin. J. Chem.*, 2015, **33**, 335–338.
57 N. L. Strutt, R. S. Forgan, J. M. Spruell, Y. Y. Botros and J. F. Stoddart, *J. Am. Chem. Soc.*, 2011, **133**, 5668–5671.
58 K. Han, Y. Zhang, J. Li, Y. Yu, X. Jia and C. Li, *Eur. J. Org. Chem.*, 2013, 2057–2060.
59 F. D'Anna, C. Rizzo, P. Vitale, S. Marullo and F. Ferrante, *New J. Chem.*, 2017, **41**, 12490–12505.
60 C. Li, Q. Xu, J. Li, F. Yao and X. Jia, *Org. Biomol. Chem.*, 2010, **8**, 1568–1576.
61 X. Shu, S. Chen, J. Li, Z. Chen, L. Weng, X. Jia and C. Li, *Chem. Commun.*, 2012, **48**, 2967–2969.
62 P. Demay-Drouhard, K. Du, K. Samanta, X. Wan, W. Yang, R. Srinivasan, A. C.-H. Sue and H. Zuilhof, *Org. Lett.*, 2019, **21**, 3976–3980.
63 N. L. Strutt, H. Zhang, S. T. Schneebeli and J. F. Stoddart, *Acc. Chem. Res.*, 2014, **47**, 2631–2642.
64 S. Sun, X.-Y. Hu, D. Chen, J. Shi, Y. Dong, C. Lin, Y. Pan and L. Wang, *Polym. Chem.*, 2013, **4**, 2224.
65 Q. Lin, Y.-Q. Fan, G.-F. Gong, P.-P. Mao, J. Wang, X.-W. Guan, J. Liu, Y.-M. Zhang, H. Yao and T.-B. Wei, *ACS Sustainable Chem. Eng.*, 2018, **6**, 8775–8781.
66 Y. Mei, Q.-W. Zhang, Q. Gu, Z. Liu, X. He and Y. Tian, *J. Am. Chem. Soc.*, 2022, **144**, 2351–2359.
67 R. R. Kothur, B. A. Patel and P. J. Cragg, *Chem. Commun.*, 2017, **53**, 9078–9080.
68 X. Tan, X. Liu, W. Zeng, Z. Zhang, T. Huang, L. Yu and G. Zhao, *Spectrochim. Acta, Part A*, 2019, **221**, 117176.
69 N. Laggoune, F. Delattre, J. Lyskawa, F. Stoffelbach, J. M. Guigner, S. Ruellan, G. Cooke and P. Woisel, *Polym. Chem.*, 2015, **6**, 7389–7394.
70 J. Chang, Q. Zhao, Le Kang, H. Li, M. Xie and X. Liao, *Macromolecules*, 2016, **49**, 2814–2820.
71 C. Huang, H. Zhang, Z. Hu, Y. Zhang and X. Ji, *Gels*, 2022, **8**(8), 475.
72 Q. Zhang, L.-L. Fan, T.-J. Yue, Z.-G. Hu, N. Li, J. Li, Y.-Q. Jiang, K.-Q. Li and H.-M. Guo, *Macromol. Chem. Phys.*, 2022, 2200253.
73 Y. Cheng, X. Lv, B. Liang, X. Wei, P. Wang and D. Xia, *Polym. Chem.*, 2023, **14**, 191–200.
74 L. Sheng, H. Liu, Z. Hu and X. Ji, *Chemistry*, 2023, **29**, e202300990.
75 C. D. Vo, D. Kuckling, H.-J. P. Adler and M. Schönhoff, *Colloid Polym. Sci.*, 2002, **280**, 400–409.
76 D. Roy and B. S. Sumerlin, *Macromol. Rapid Commun.*, 2014, **35**, 174–179.
77 M. Seuss, W. Schmolke, A. Drechsler, A. Fery and S. Seiffert, *ACS Appl. Mater. Interfaces*, 2016, **8**, 16317–16327.
78 W. Schmolke, M. Ahmadi and S. Seiffert, *Phys. Chem. Chem. Phys.*, 2019, **21**, 19623–19638.
79 J. Li, X. Yu, A. Herberg and D. Kuckling, *Macromol. Rapid Commun.*, 2019, **40**, e1800674.
80 L. D. Taylor, H. S. Kolesinski, A. C. Mehta, L. Locatell and P. S. Larson, *Makromol. Chem., Rapid Commun.*, 1982, **3**, 779–782.
81 M. W. Jones, S.-J. Richards, D. M. Haddleton and M. I. Gibson, *Polym. Chem.*, 2013, **4**, 717–723.
82 A. Guyomard, D. Fournier, S. Pascual, L. Fontaine and J.-F. Bardeau, *Eur. Polym. J.*, 2004, **40**, 2343–2348.
83 H. T. Ho, M. E. Levere, D. Fournier, V. Montembault, S. Pascual and L. Fontaine, *Aust. J. Chem.*, 2012, **65**, 970.
84 C. M. Gardner, C. E. Brown and H. D. H. Stöver, *J. Polym. Sci., Part A: Polym. Chem.*, 2012, **50**, 4674–4685.
85 F. François, C. Nicolas, G. Forcher, L. Fontaine and V. Montembault, *Eur. Polym. J.*, 2020, **141**, 110081.
86 L. Jia, S. M. Kilbey and X. Wang, *Langmuir*, 2020, **36**, 10200–10209.
87 M. E. Levere, H. T. Ho, S. Pascual and L. Fontaine, *Polym. Chem.*, 2011, **2**, 2878.
88 S. Pascual, T. Blin, P. J. Saikia, M. Thomas, P. Gosselin and L. Fontaine, *J. Polym. Sci., Part A: Polym. Chem.*, 2010, **48**, 5053–5062.
89 X. Yu, A. Herberg and D. Kuckling, *Eur. Polym. J.*, 2019, **120**, 109207.
90 G. Wang, H. Qiang, Y.-Z. Guo, J. Yang, K. Wen and W.-B. Hu, *Org. Biomol. Chem.*, 2019, **17**, 4600–4604.
91 L. Wu, C. Han, X. Jing and Y. Yao, *Chin. Chem. Lett.*, 2021, **32**, 3322–3330.
92 C. Schönbeck, H. Li, B.-H. Han and B. W. Laursen, *J. Phys. Chem. B*, 2015, **119**, 6711–6720.
93 P. Thordarson, *Chem. Soc. Rev.*, 2011, **40**, 1305–1323.
94 P. Thordarson, in *Supramolecular chemistry*, ed. J. W. Steed and P. A. Gale, Wiley, Chichester, 2012.
95 K. Hirose, *J. Inclusion Phenom. Macrocyclic Chem.*, 2001, **39**, 193–209.
96 L. Alderighi, P. Gans, A. Ienco, D. Peters, A. Sabatini and A. Vacca, *Coord. Chem. Rev.*, 1999, **184**, 311–318.
97 C. Li, L. Zhao, J. Li, X. Ding, S. Chen, Q. Zhang, Y. Yu and X. Jia, *Chem. Commun.*, 2010, **46**, 9016–9018.
98 M. Boominathan and M. Arunachalam, *ACS Appl. Polym. Mater.*, 2020, **2**, 4368–4372.
99 M. Boominathan, J. Kiruthika and M. Arunachalam, *J. Polym. Sci., Part A: Polym. Chem.*, 2019, **57**, 1508–1515.
100 M. P. Foster, C. A. McElroy and C. D. Amero, *Biochemistry*, 2007, **46**, 331–340.
101 C. Li, S. Chen, J. Li, K. Han, M. Xu, B. Hu, Y. Yu and X. Jia, *Chem. Commun.*, 2011, **47**, 11294–11296.
102 M. E. Harmon, D. Kuckling, P. Pareek and C. W. Frank, *Langmuir*, 2003, **19**, 10947–10956.

103 M. E. Harmon, D. Kuckling and C. W. Frank, *Macromolecules*, 2003, **36**, 162–172.
104 D. J. Anderson, *Clin. Chem.*, 1989, **35**, 2152–2153.
105 E. G. Sheetz, D. van Craen and A. H. Flood, in *Anion-binding catalysis*, ed. O. García Mancheño, Wiley–VCH GmbH, 2022, pp. 79–109.
106 D. A. Stauffer, R. E. Barrans and D. A. Dougherty, *J. Org. Chem.*, 1990, **55**, 2762–2767.
107 J. C. Adrian and C. S. Wilcox, *J. Am. Chem. Soc.*, 1991, **113**, 678–680.
108 A. B. Braunschweig, C. M. Ronconi, J.-Y. Han, F. Aricó, S. J. Cantrill, J. F. Stoddart, S. I. Khan, A. J. P. White and D. J. Williams, *Eur. J. Org. Chem.*, 2006, 1857–1866.
109 L. Li and G. J. Clarkson, *Org. Lett.*, 2007, **9**, 497–500.
110 T. Boinski and A. Szumna, *Tetrahedron*, 2012, **68**, 9419–9422.
111 Z. Zhang, B. Xia, C. Han, Y. Yu and F. Huang, *Org. Lett.*, 2010, **12**, 3285–3287.
112 Y. Ma, Z. Zhang, X. Ji, C. Han, J. He, Z. Abliz, W. Chen and F. Huang, *Eur. J. Org. Chem.*, 2011, 5331–5335.
113 T. Ogoshi, K. Demachi, K. Kitajima and T. Yamagishi, *Chem. Commun.*, 2011, **47**, 7164–7166.
114 Y. Chen, M. He, B. Li, L. Wang, H. Meier and D. Cao, *RSC Adv.*, 2013, **3**, 21405.
115 J. Han, X. Hou, C. Ke, H. Zhang, N. L. Strutt, C. L. Stern and J. F. Stoddart, *Org. Lett.*, 2015, **17**, 3260–3263.
116 D. N. Shurpik and I. I. Stoikov, *Russ. J. Gen. Chem.*, 2016, **86**, 752–755.